

Medical Biophysics: ocular flow, cancer growth, heart electrophysiology

Jean Bragard

Department of Physics and Applied Mathematics,

&

*Institute of Data Science and Artificial Intelligence,
University of Navarra.*

31008 Pamplona. SPAIN.

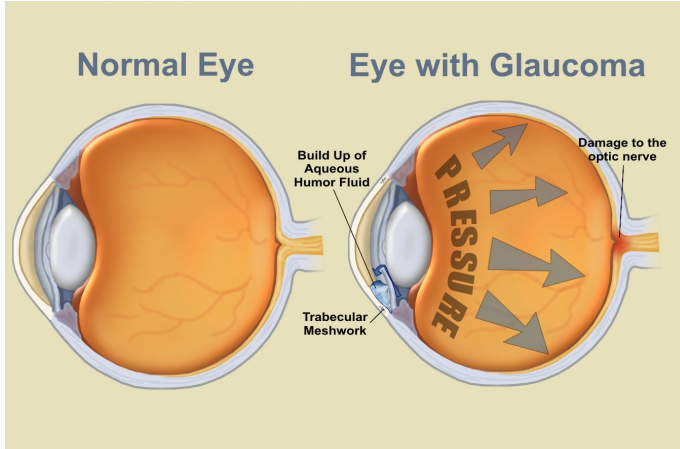


Program:

- i) Fluid flow in the eye
- ii) Tumor growth dynamics
- iii) Atrial fibrillation
- iv) Wave propagation in the heart

I) Fluid flow in the eye

Glaucoma: “the silent thief of sight”



No symptoms

No pain

Half of the people are undiagnosed

Prevalence around 100 Million people.

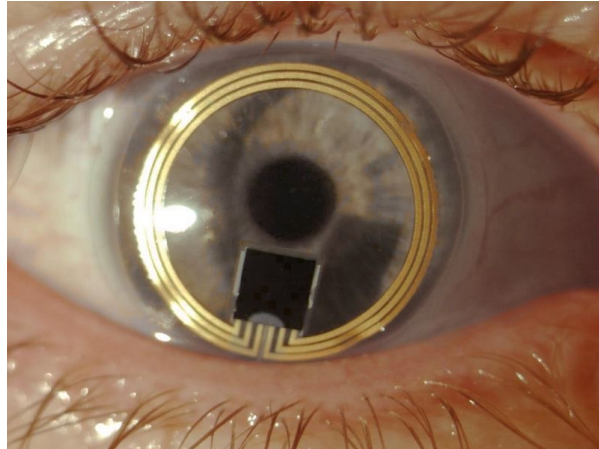
Main culprit is the high eye pressure.

Intraocular pressure (IOP).

Glaucoma damages vision by destroying the optic nerve.

Your peripheral vision is lost first.

Measuring the IOP continuously

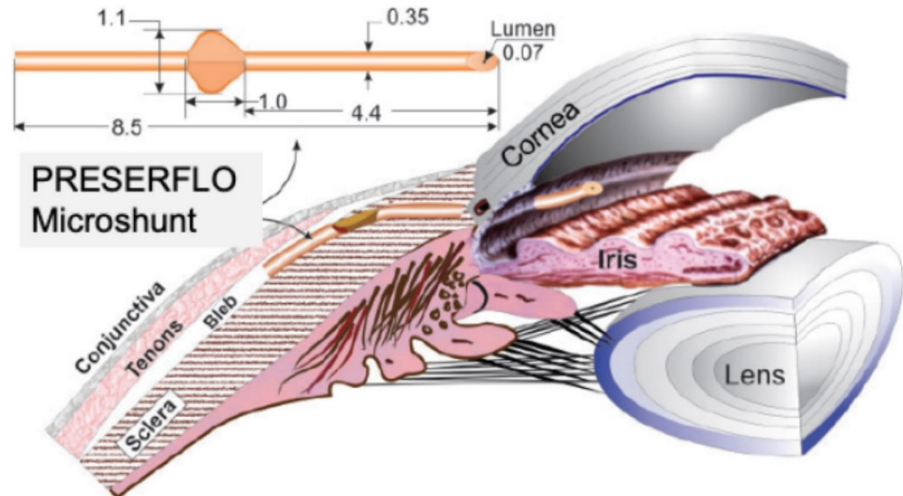
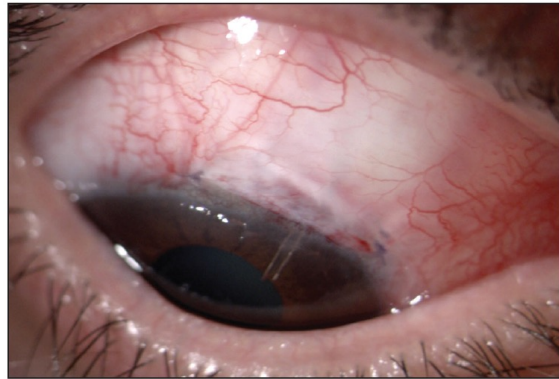


A **MEMS sensor** includes a circular active outer ring and passive strain gauges to measure corneal curvature changes in response to IOP. (Sensimed AG™).

A **normal eye** maintains a positive IOP in the range of 10 to 22 mmHg. Abnormal elevation (>22 mmHg) and fluctuation of IOP are considered the main risk factors for glaucoma.

Treatment focuses on reducing IOP either mechanically (laser, surgery, shunts) or chemically (medication such as IOP-reducing eye drops).

Reduction of the IOP through the insertion of a drainage device



The drainage reduces the IOP.

If the drainage is too large there is a risk of severe hypotony (postoperative).

We evaluate the flow characteristics of the PRESERFLO Microshunt.

tvst

Article

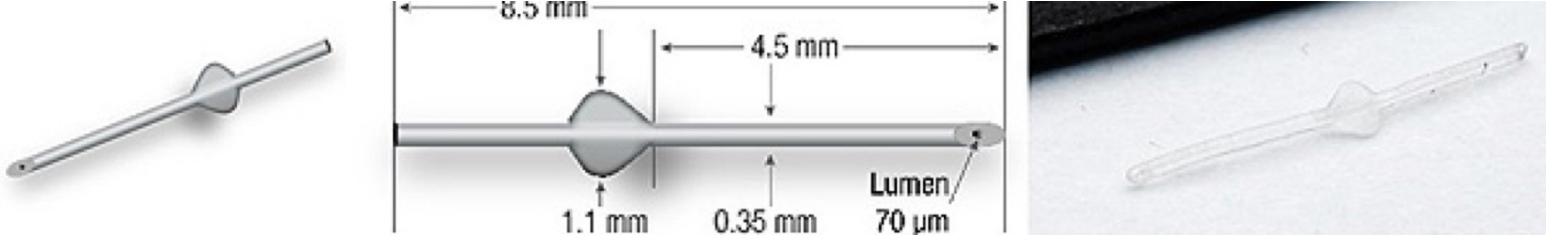
Evaluation of the Ultrastructural and In Vitro Flow Properties of the PRESERFLO MicroShunt

Marta Ibarz Barberá^{1,2}, Jose Luis Hernández-Verdejo³, Jean Bragard⁴, Javier Burguete⁴, Laura Morales Fernández^{5,6}, Pedro Tañá Rivero⁷, Rosario Gómez de Liaño⁵, and Miguel A. Teus⁸⁻¹⁰

Colabora. M. I. Barberá, MD., PhD.,

Transl Vis Sci Technol. 2021;10(13):26, <https://doi.org/10.1167/tvst.10.13.26>

Preserflo: longitud 8,5 mm, diámetro interno 70 micras



Características implante Preserflo:

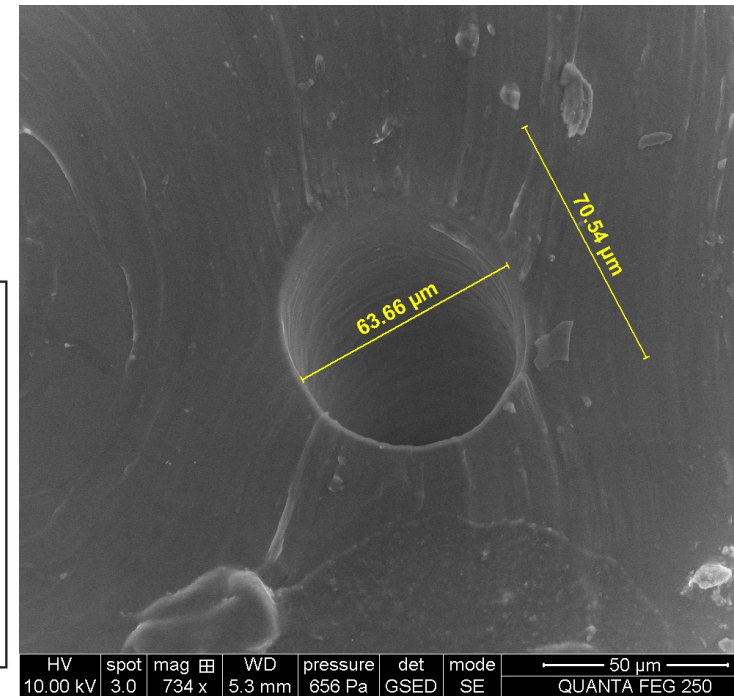
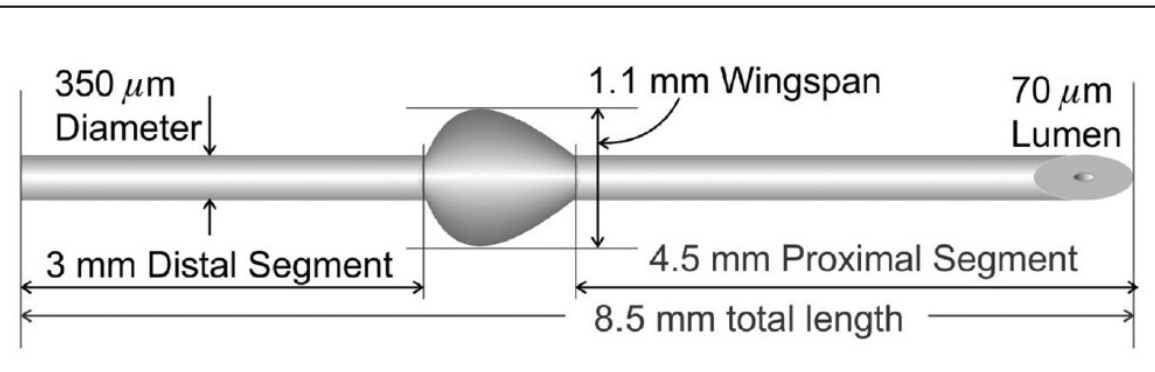
Longitud: 8,5 mm

Lumen: 70 micras

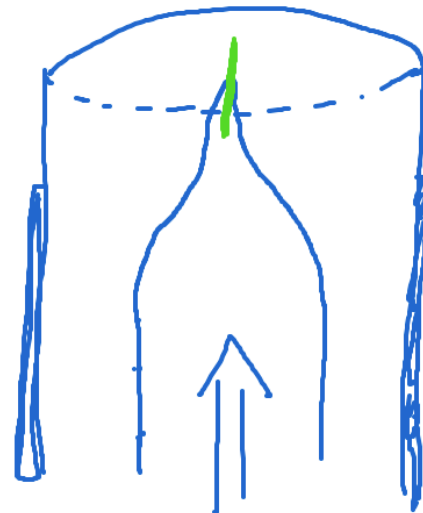
Diámetro externo: 350 micras.

Resistencia al flujo: $R = 1,30 \text{ (mmHg}/(\mu\text{L/min})$

Flujo de humor acuoso: 2 microL/min

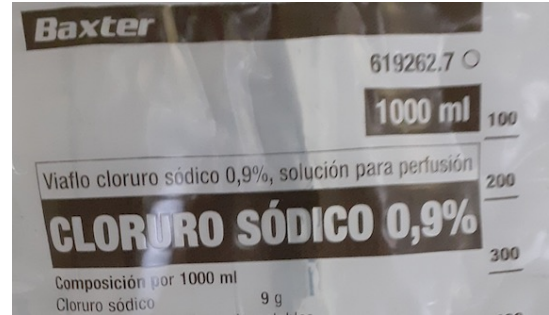
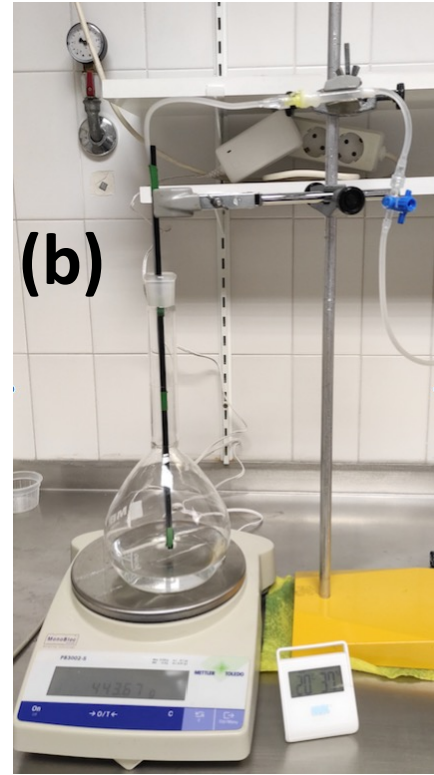


Experimental sketch and realization



Parafilm® M sealing film





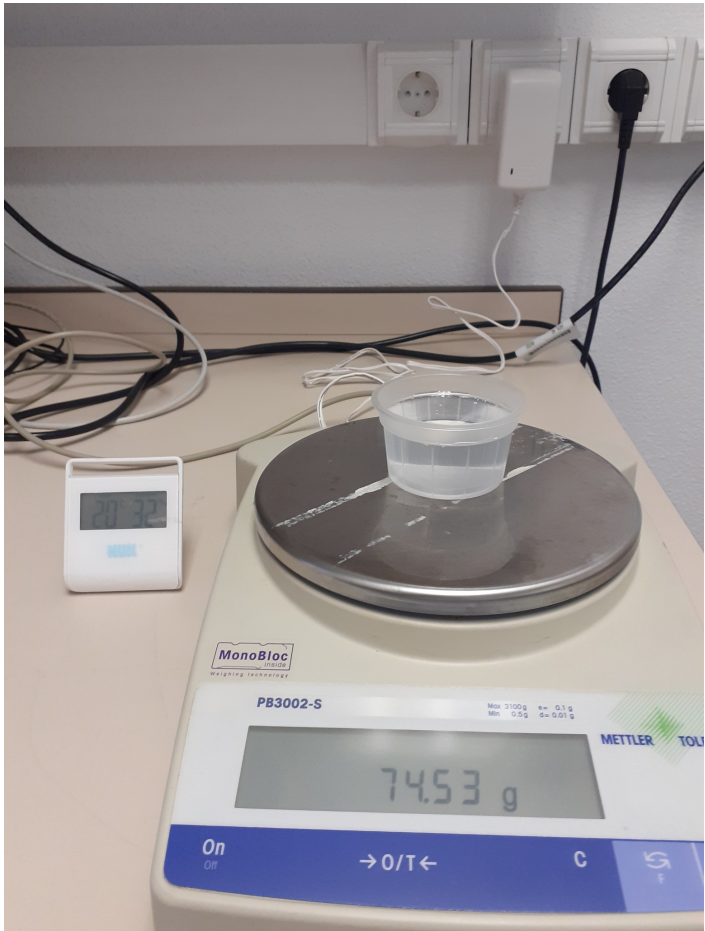
Gravity-driven flow setup

Experimental caveats

- Bubbles*
- Evaporation



Evaporation

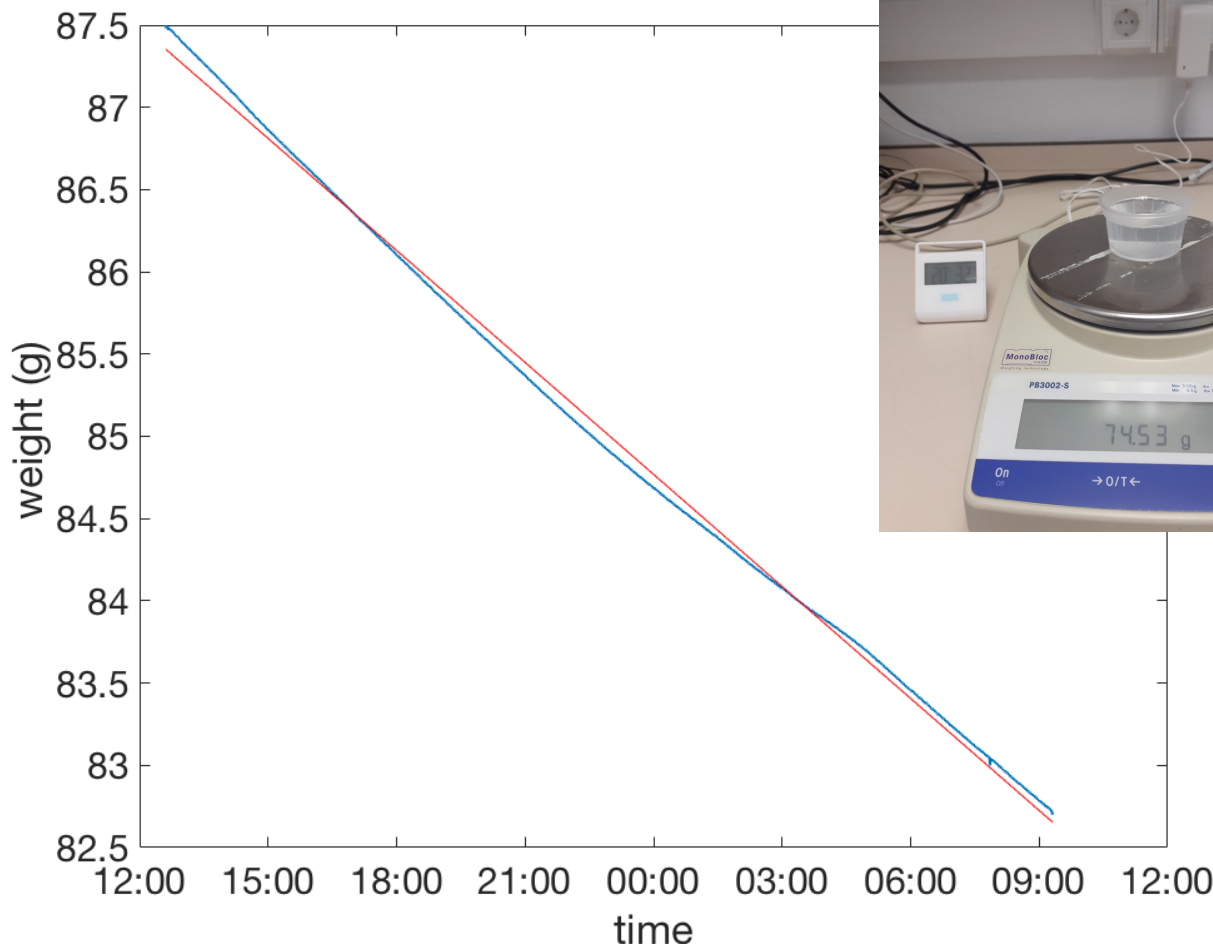


Open to air, the container is loosing mass through evaporation.

By monitoring the weight we can estimate the Evaporation rate.

$T \approx 20 \text{ }^{\circ}\text{C}$, humidity in [32-37]%

Evaporation (I)

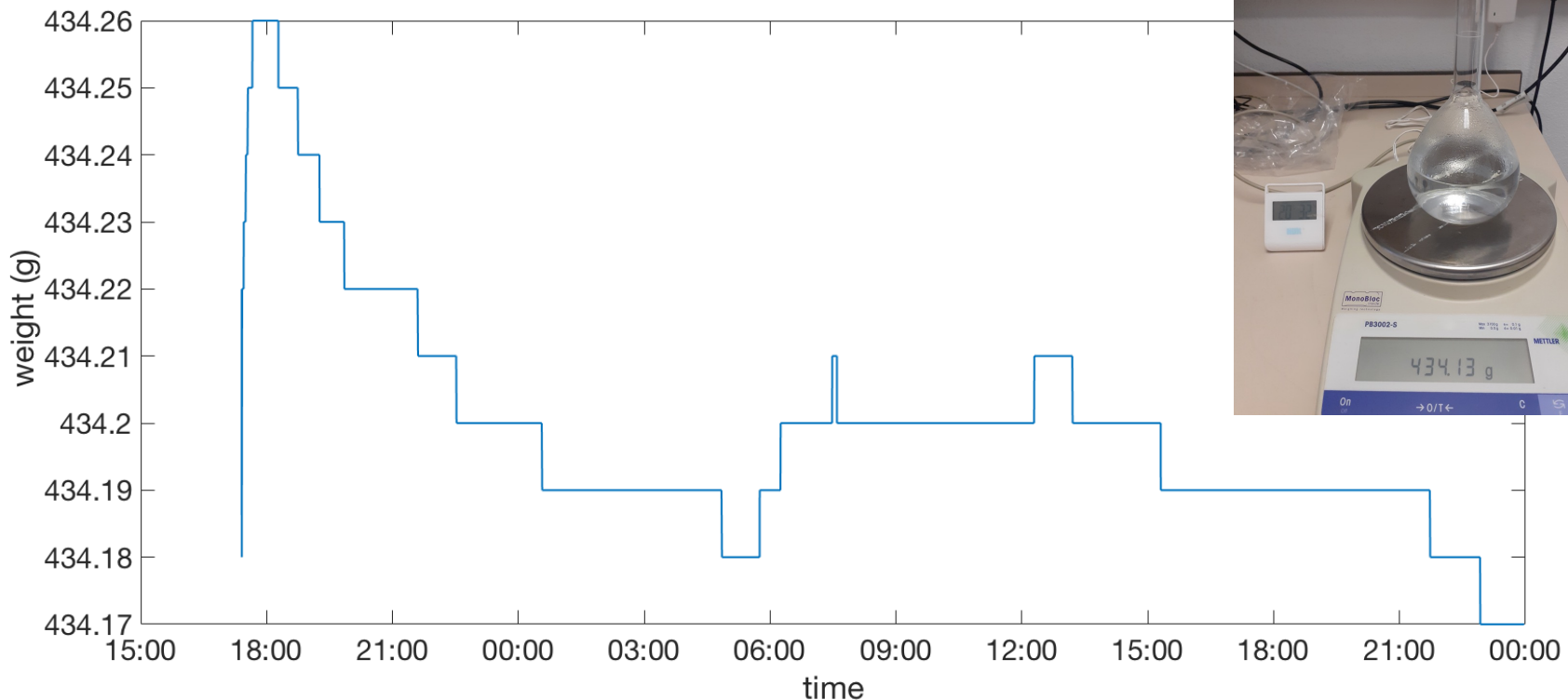


Total evaporation: -5.448 g/(24h)

Evaporation by unit area: -0.1864 g/(24h cm²)

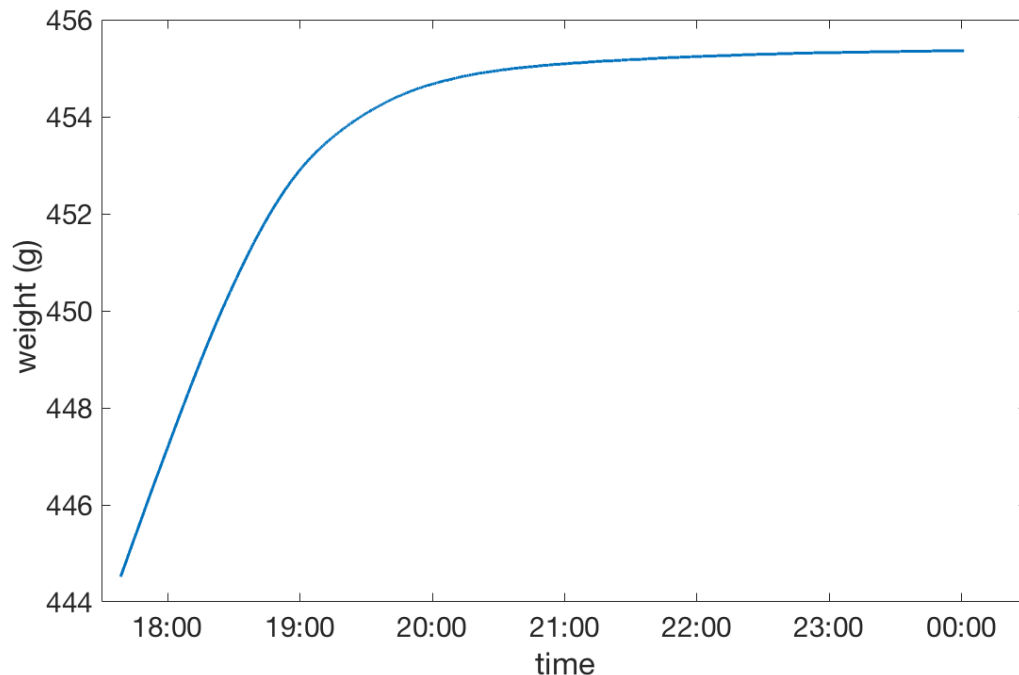
$$D = 6.1 \text{ cm}$$
$$A = 29.2 \text{ cm}^2$$

Evaporation (II)



Using a volumetric flask the evaporation is negligible

Bubbles !



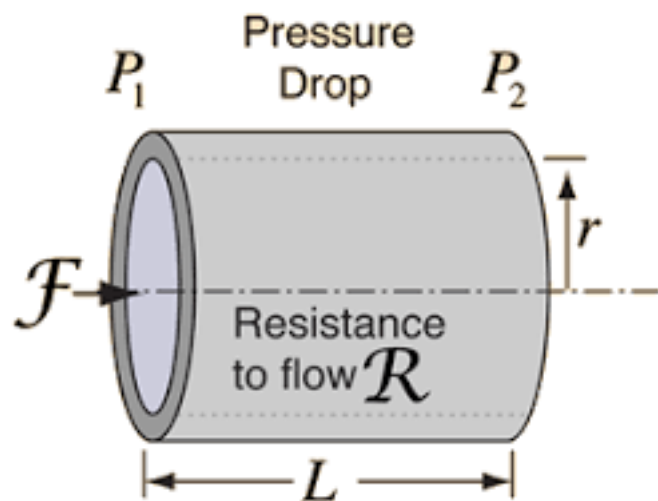
Problem : bubbles are stopping the flow !

Poiseuille flow

$$Q = \frac{\pi r^4 \Delta p}{8\mu L}$$

$$\Delta p = p_1 - p_2 \quad \text{Pressure drop}$$

L Length of the device



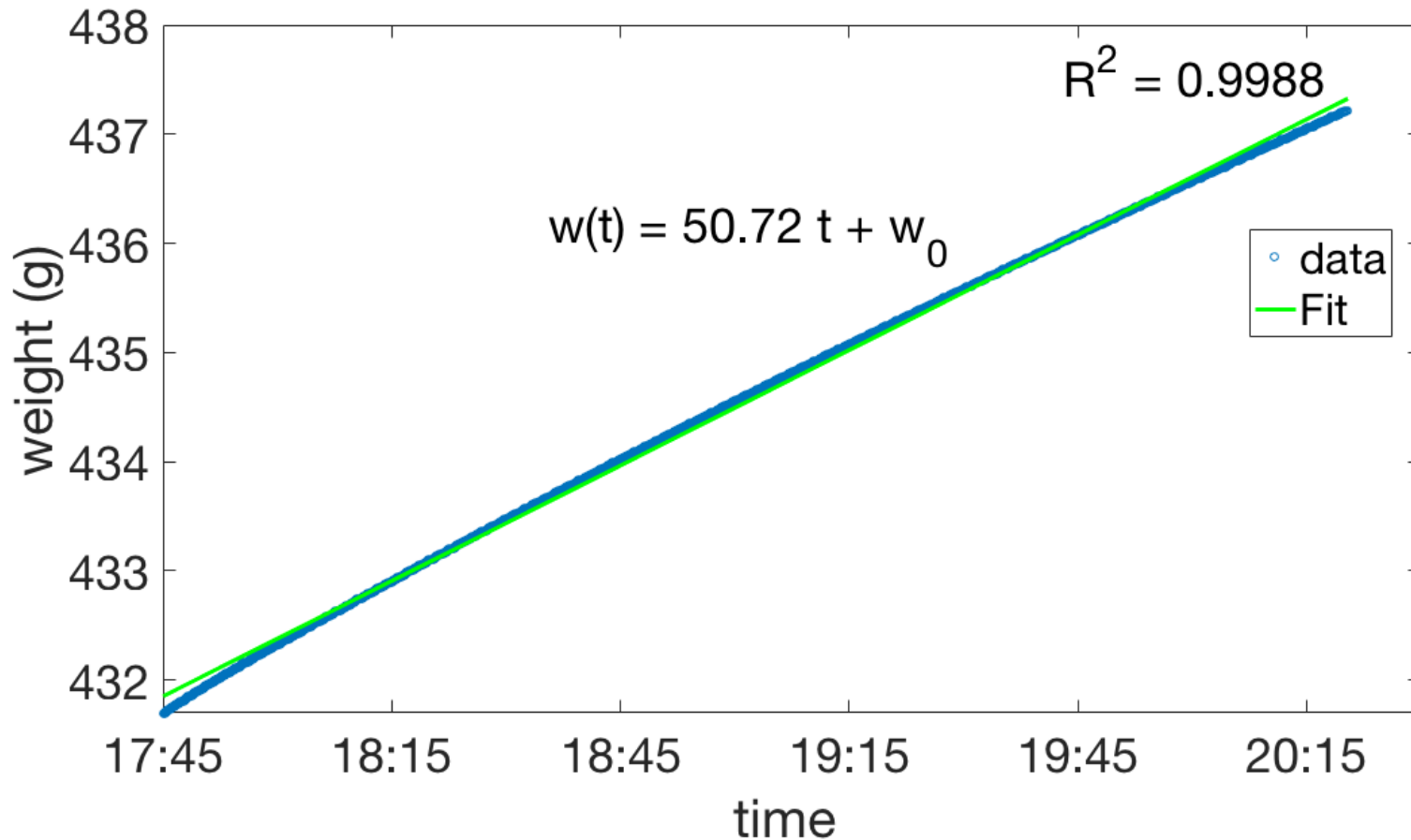
r Radius of the device

μ Dynamical viscosity

Q Flow (volume/time)

For the Preserflo device, we compute the following: $Q\left(\frac{\text{g}}{\text{day}}\right) = 0.601\Delta h(\text{cm})$

Poiseuille flow (Results i)

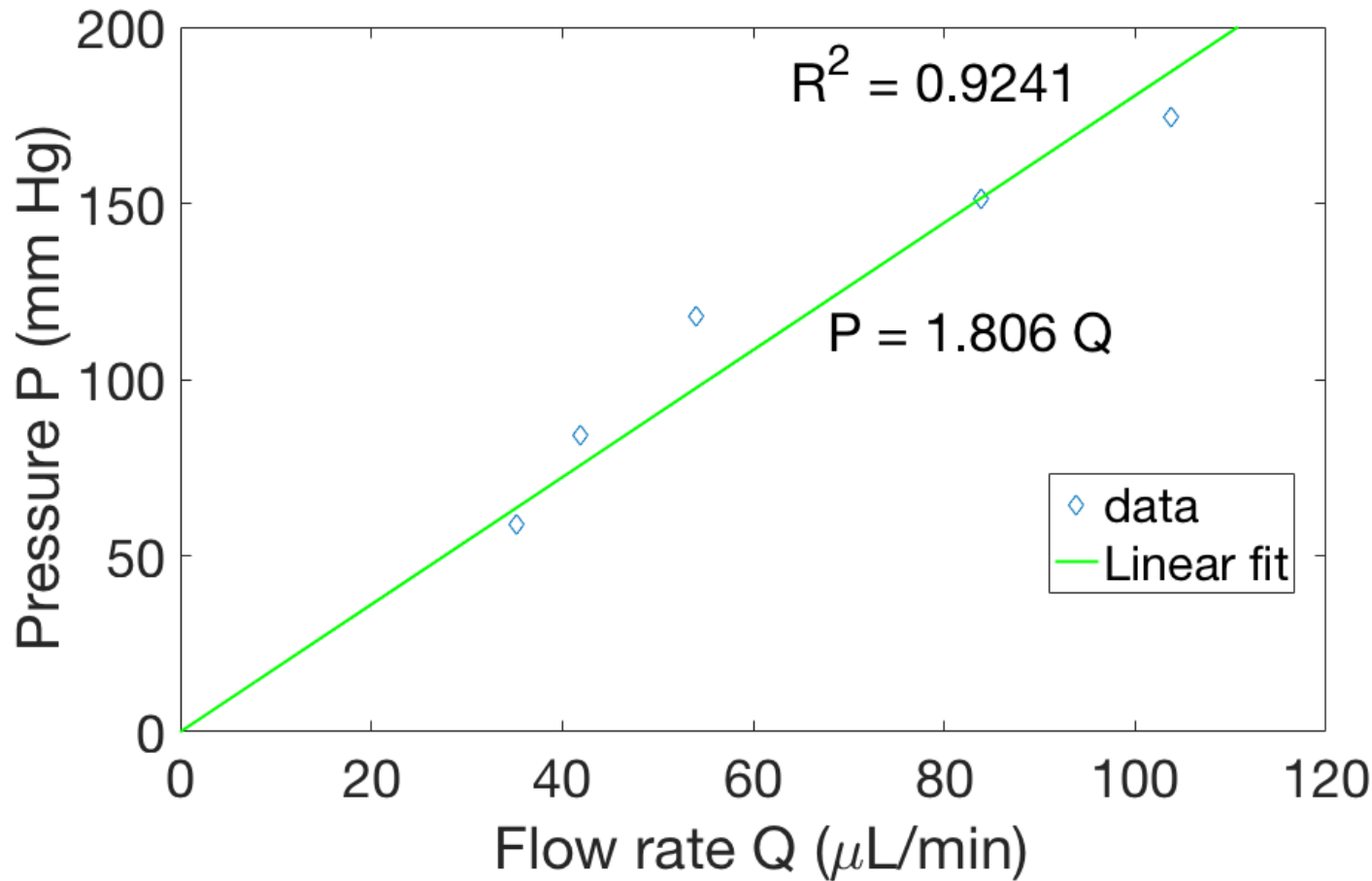


Here $\Delta h=80.1$ cm

$$Q_{\text{theo.}} = 48.10 \left(\frac{\text{g}}{\text{day}} \right)$$

t is measured in day

Poiseuille flow (Collecting results)



Theoretically: $P = 1.7626 Q$

$\mu = 0.9775 \text{ cP}$

Conclusions

- The **gravity-flow experiment** allowed us to measure the experimental resistance to flow, which was $RE = 1.33^*$ mmHg/(μ L/min), 95%CI (1.15;1.50) in agreement with the theoretical resistance to flow R given by the Hagen-Poiseuille equation.
- The experimental and theoretical flow testing showed that the pressure drop across this device would not be large enough to avoid hypotony.
- The fluid properties of glaucoma subconjunctival drainage devices determine their specific bleb-forming capacity and ability to avoid hypotony and therefore their safety and efficacy profile.

$$\mu = 0.7185 \text{ cP} \quad (*\text{aqueous humor})$$

II) Tumor growth dynamics

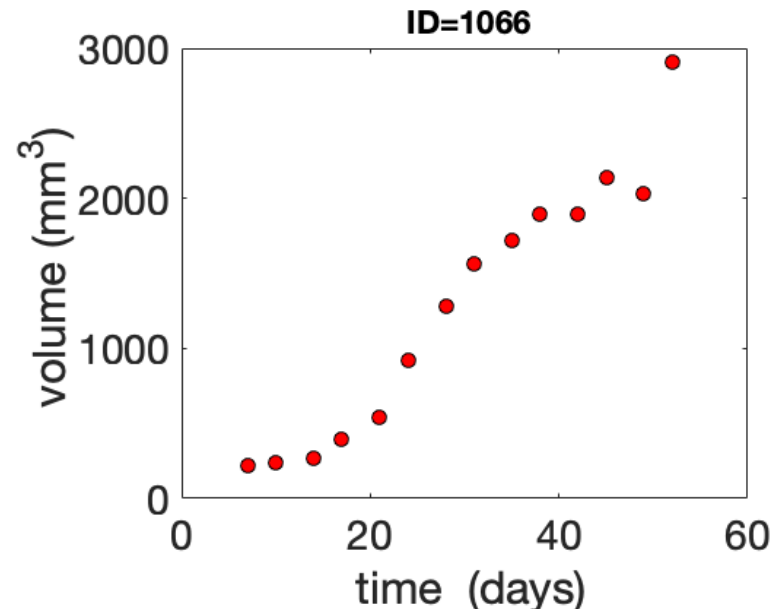
Tumor growth modeling (TGM)



We have access to numerous data of the tumor's evolution.
The tumor volume is measured by a caliper technique over time.

Interest of the model for

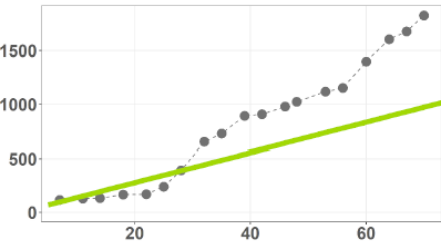
1. Disease (unperturbed tumor) progression
2. Treatment effects



TGM: “classical” models

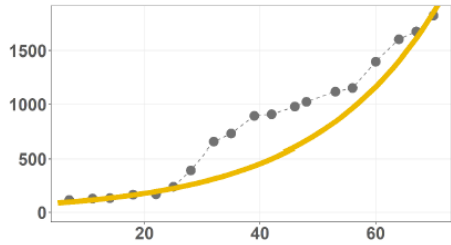
$$\frac{dTS}{dt} = \lambda$$

Lineal Model



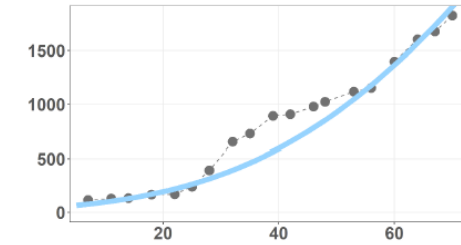
$$\frac{dTS}{dt} = \lambda \times TS$$

Exponential Model



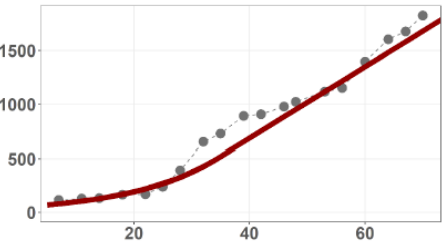
$$\frac{dTS}{dt} = \alpha \times TS \times \log\left(\frac{TS_{max}}{TS}\right)$$

Gompertz Model



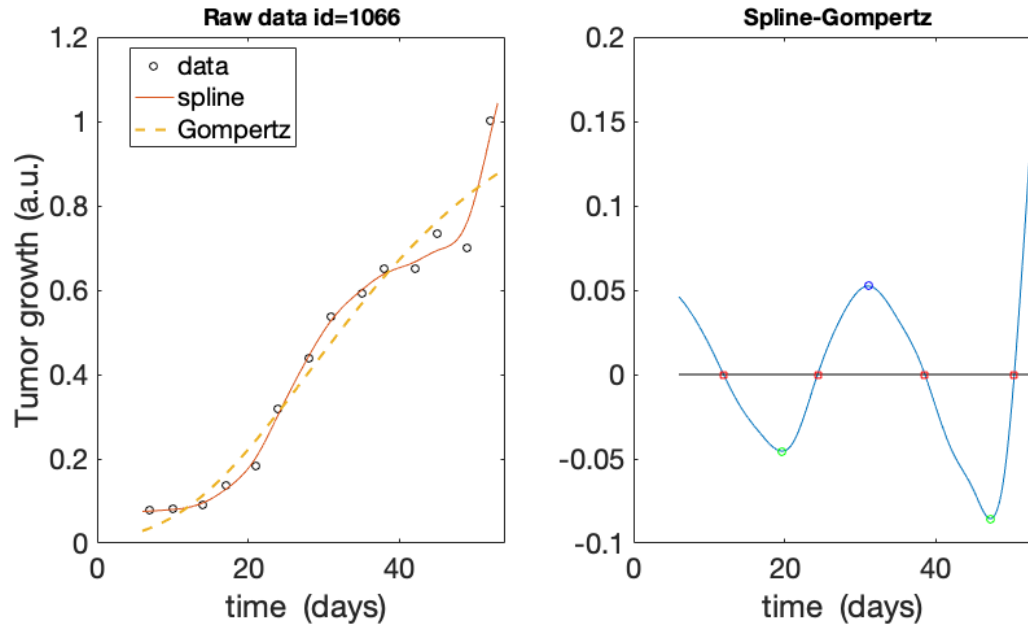
$$\frac{dTS}{dt} = \frac{\lambda_o \times TS}{\left\{1 + \left[\left(\lambda_0/\lambda_1\right) \times TS\right]^\psi\right\}^{1/\psi}}$$

Simeoni Model



Classical models for tumor growth are monotonic and the data seem to indicate that the growth could be oscillatory.

Data exploration (use splines)

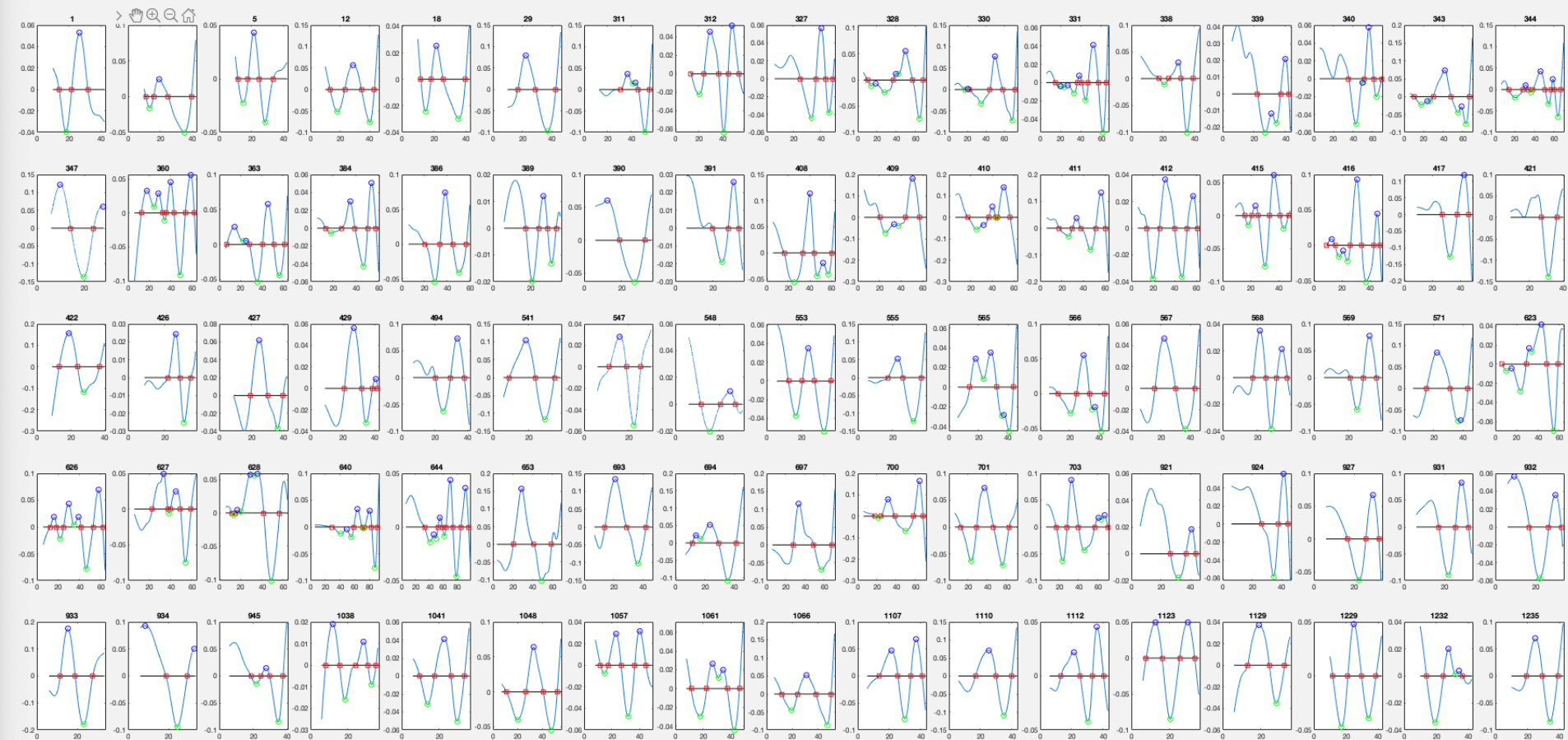


First we explore a purely empirical model based on the **cubic spline fitting** of the data.

We compare the spline with the best classical fit, i.e., logistic, exponential or Gompertz.

From the residuals, we compute the “half period” of the oscillations.

Data exploration (85 data, 6 tumor types)



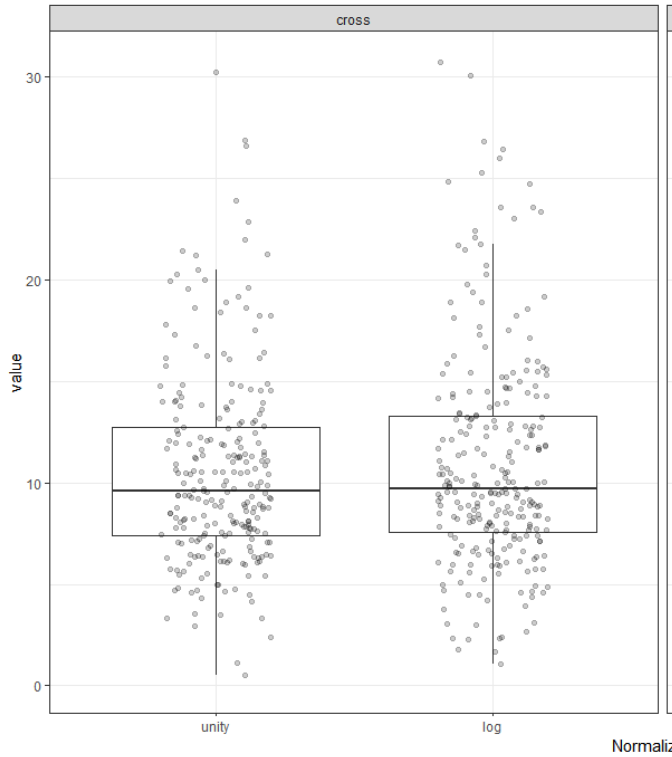
We compute the half-periods in four different ways:

Zero-crossings of residuals (when data are normalized with unity and log scale);

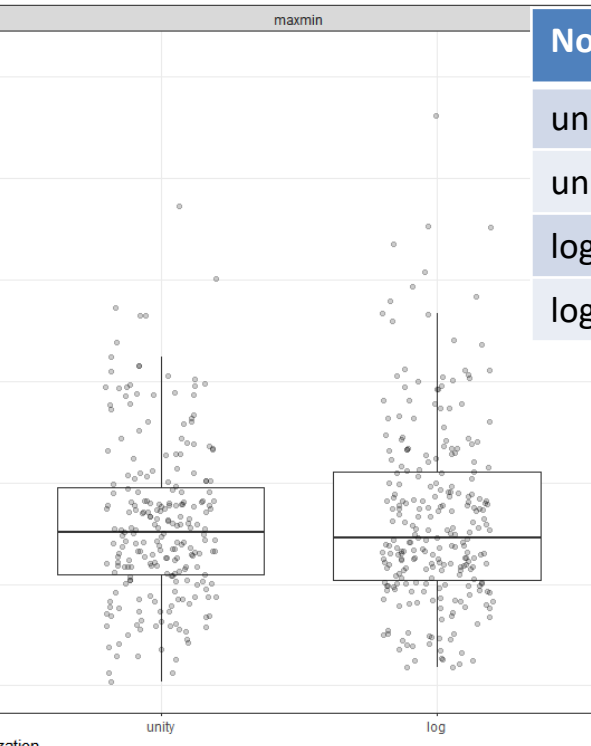
Successive extrema of the residuals (for data normalized with unity and log scale).

Empirical half periods

zero-crossings



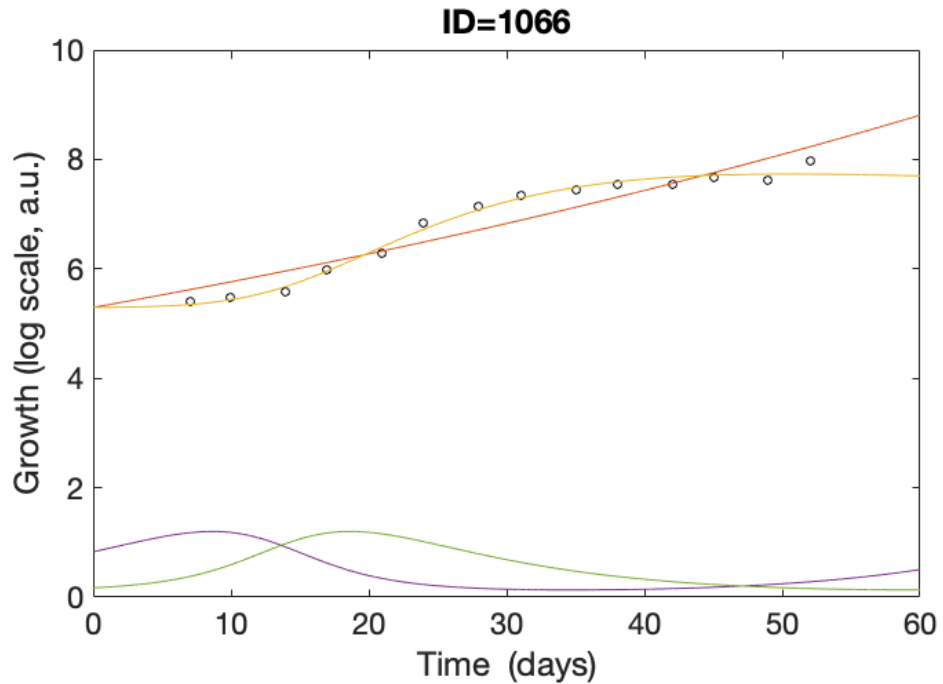
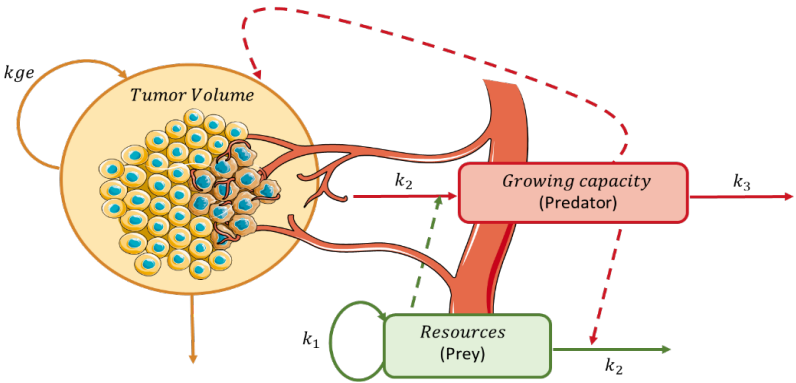
extrema



Normalization	HPs	mean	sd
unity	cross	10.5	4.72
unity	maxmin	8.00	3.95
log	cross	10.9	5.32
log	maxmin	8.25	4.47

Collecting all the available data, we observe that the median values for the half-periods are in the 8 to 10 days range.

An oscillating model for tumor growth



We combine a prey-predator model with a classical exponential growth to produce an oscillating model.

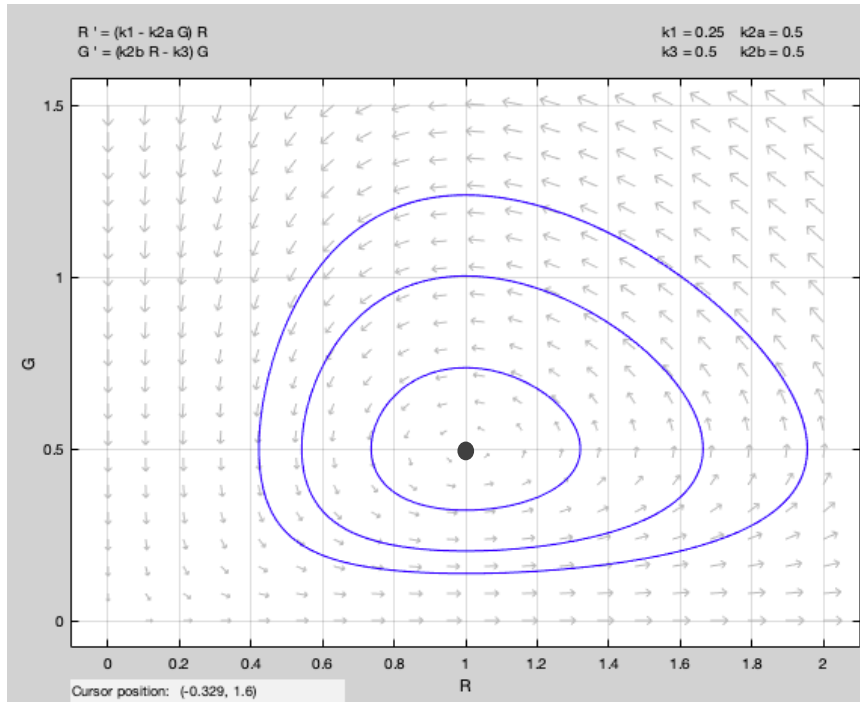
The new model (3 ODEs) is able to fit the data nicely.

$$\frac{dT}{dt} = k_{ge} T G - k_{death} T \quad \text{Tumor vol.}$$

$$\frac{dR}{dt} = k_1 R - k_2 R G \quad \text{Prey}$$

$$\frac{dG}{dt} = k_2 R G - k_3 G \quad \text{Predator}$$

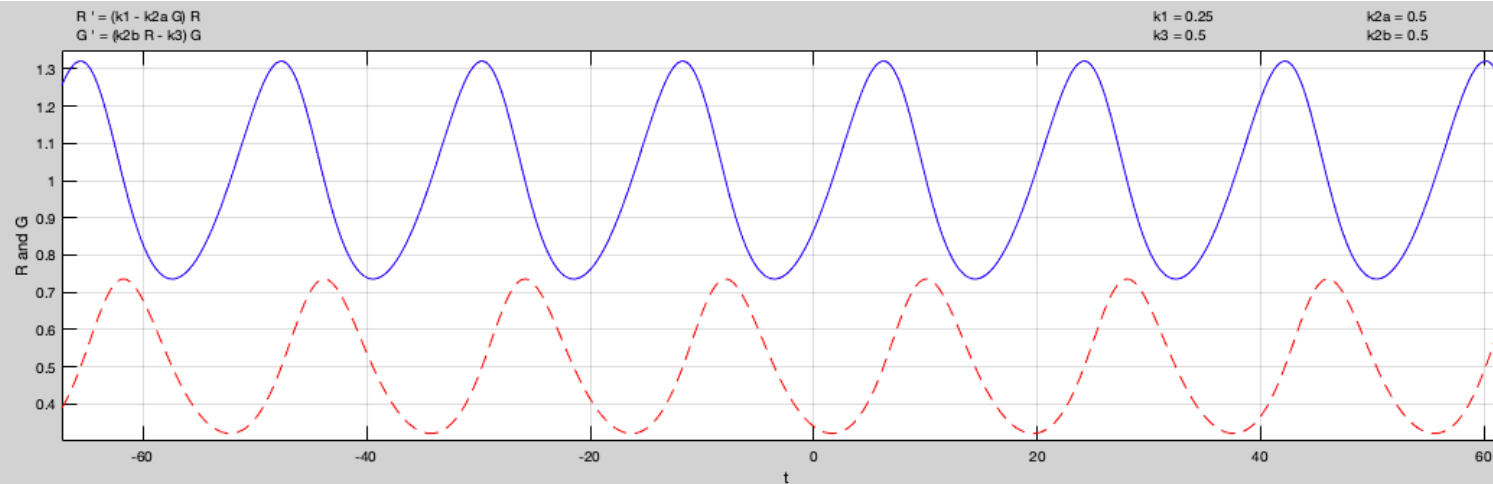
Prey (R) – Predator (G) dynamics



$$\frac{dR}{dt} = k_1 R - k_2 R G$$

$$\frac{dG}{dt} = k_2 R G - k_3 G$$

$$G_{eq} = \frac{k_1}{k_2} \quad R_{eq} = \frac{k_3}{k_2}$$

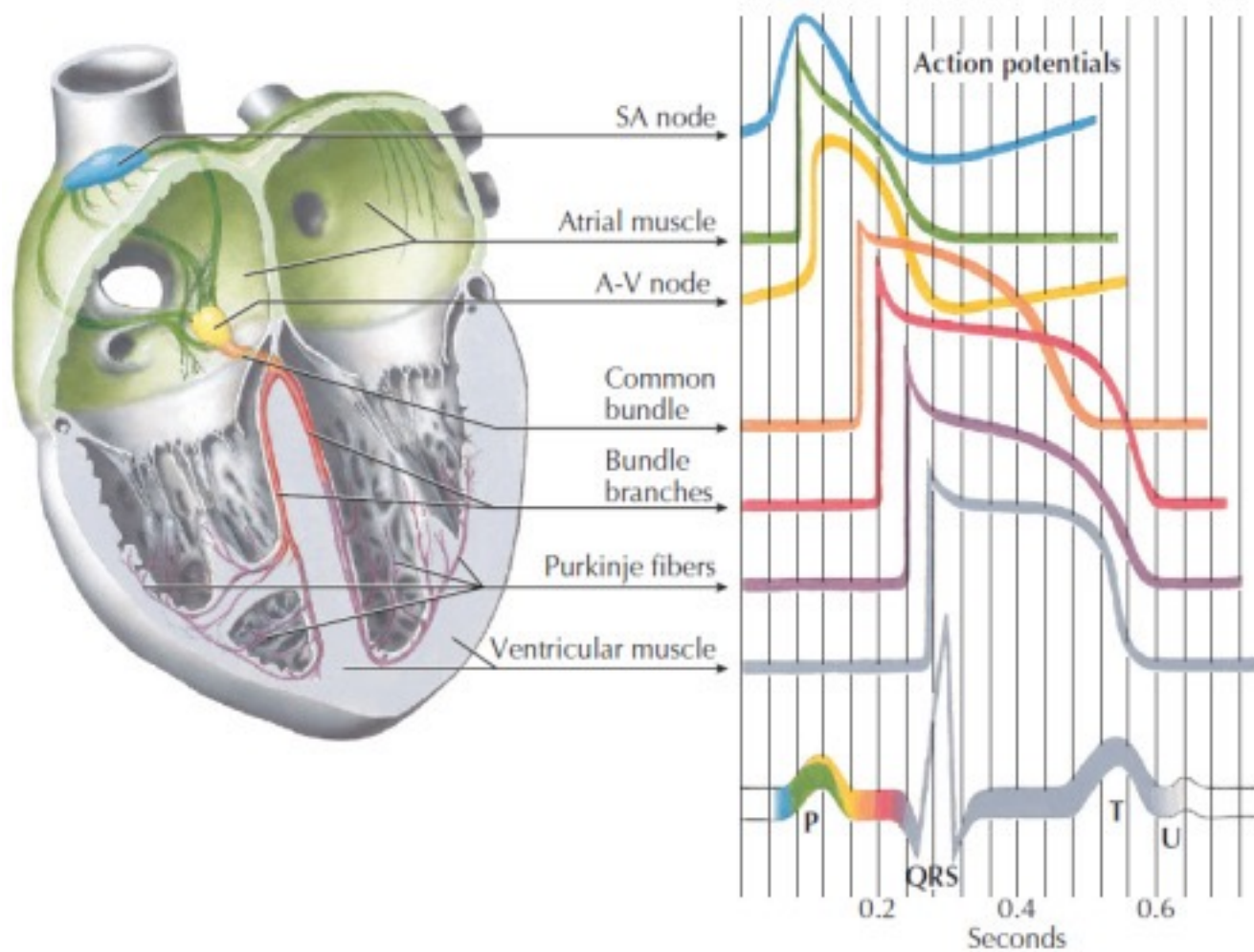


Partial conclusions

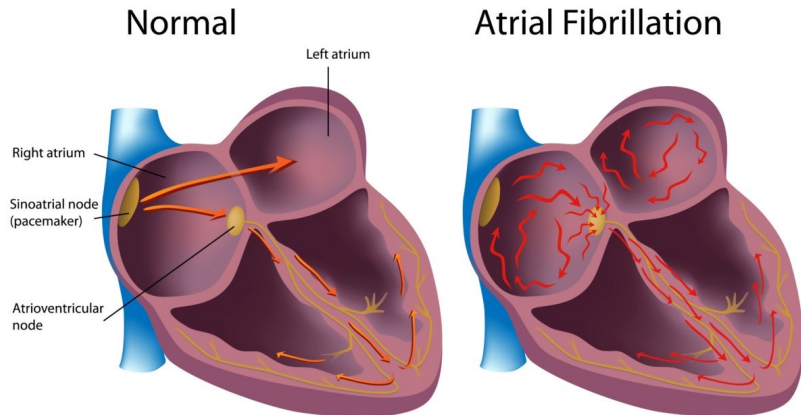
- The time evolution of tumor growth data indicates that the growth is oscillating.
- We characterize the 'half-period' of the oscillations to have median values in the range 8 to 10 days
- We provide a very simple model to account for the oscillating tumor growth behavior.
- We statistically compare the previous classical model with the proposed model.

III) Atrial fibrillation

Cardiac conduction system and its relation with the ECG



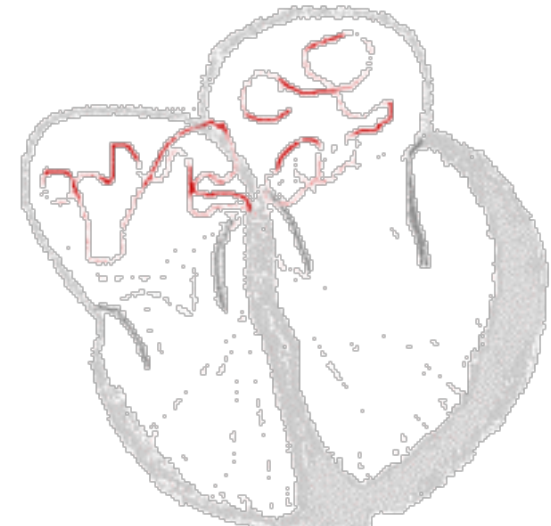
Atrial fibrillation (Afib)



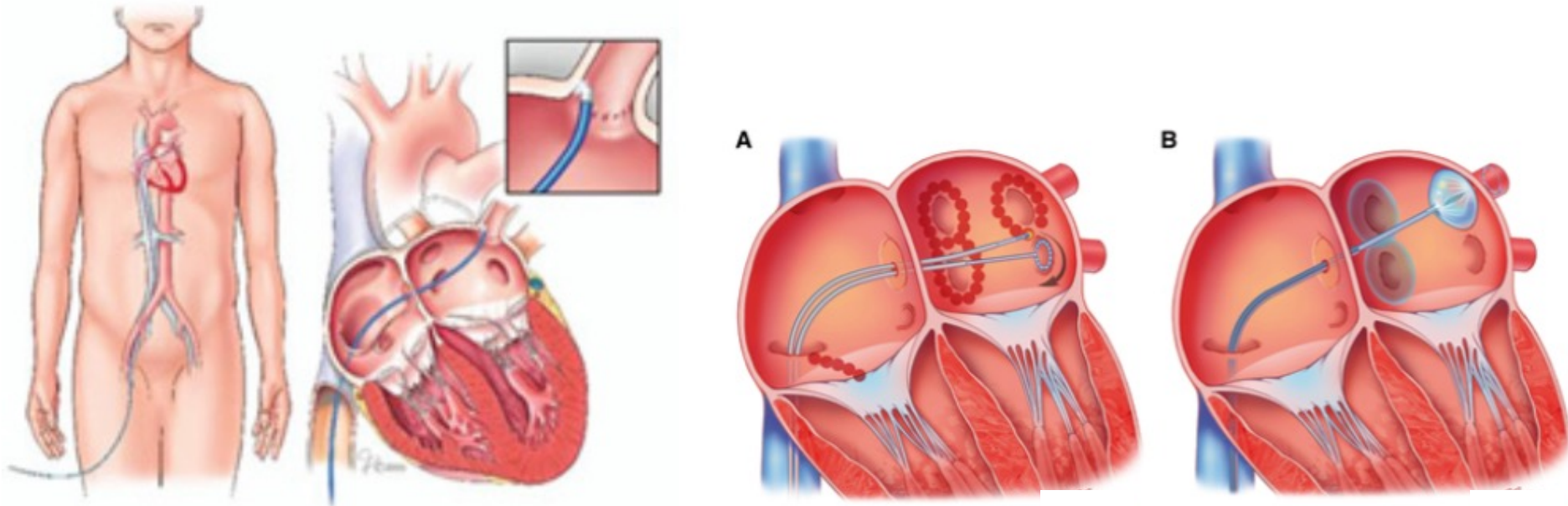
We have studied images that corresponds to Afib patients (left atrium)

1. Pathophysiology
2. Predictive power.

Afib is an arrhythmia that does not present a direct risk for the patient's life (the fluid fills the ventricles anyway). But in the long run, a thrombus may form in the atrium and sometimes travels to the brain and cause a stroke.



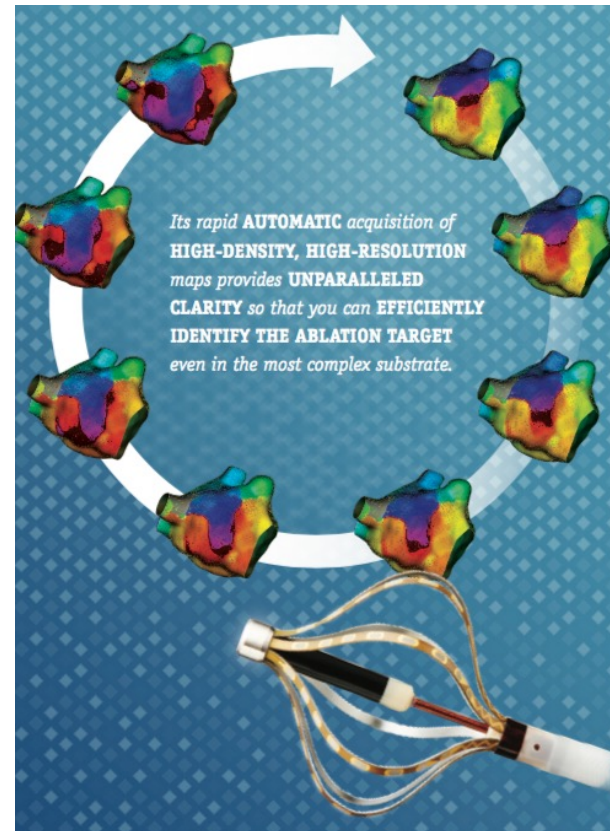
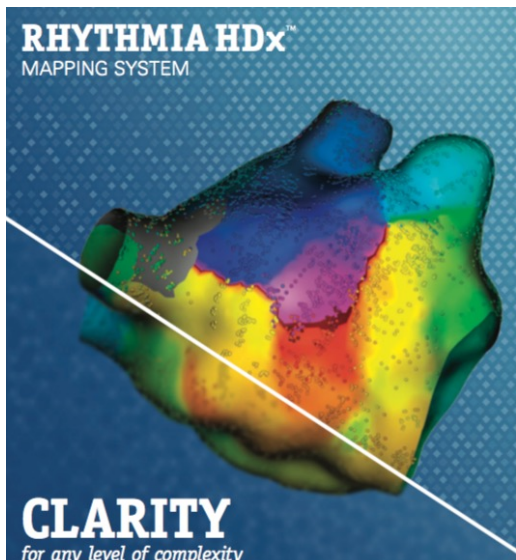
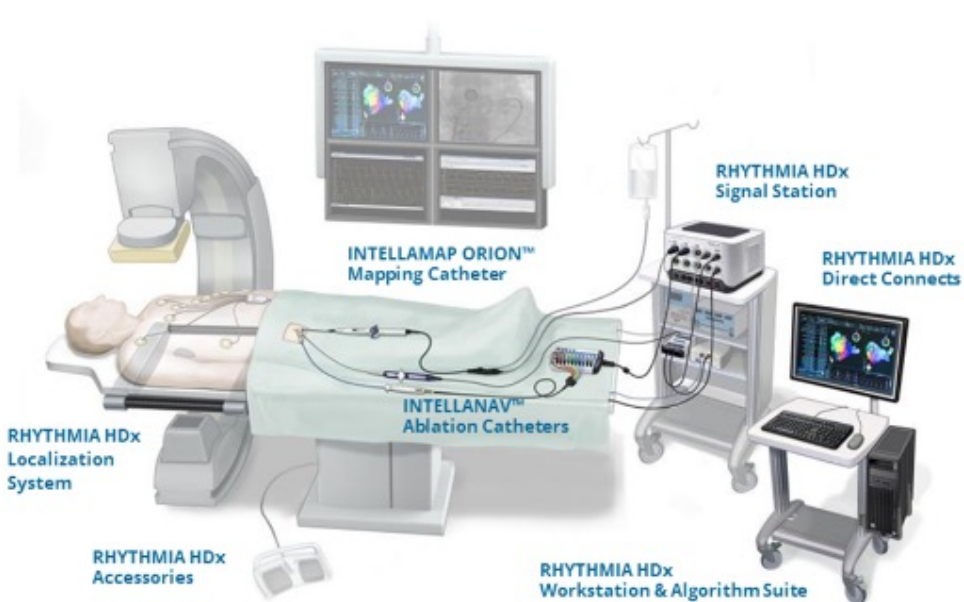
Clinical solution to Afib is to ablate the re-entry circuit and essentially the PVs



~30% of the ablation procedures will fail (Afib presents after 1 year follow-up)
Two main techniques are used: radiofrequency ablation (A) and cryoablation (B).
+Blood thinners (anticoagulation therapy) to prevent blood clots from forming.

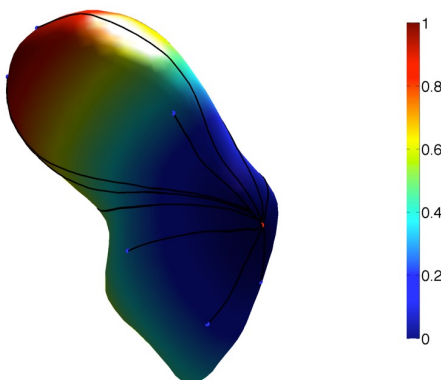
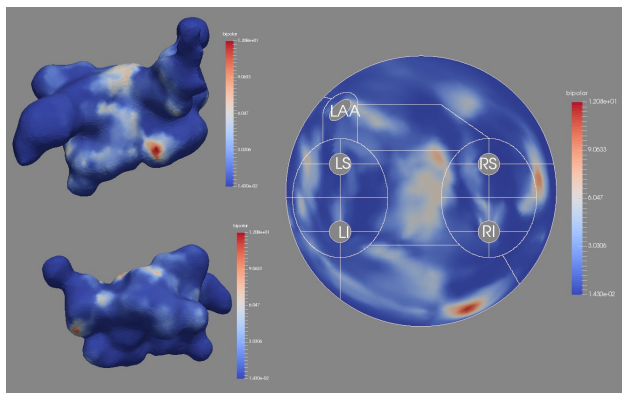
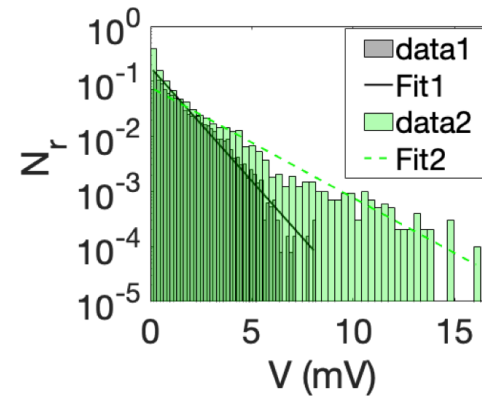
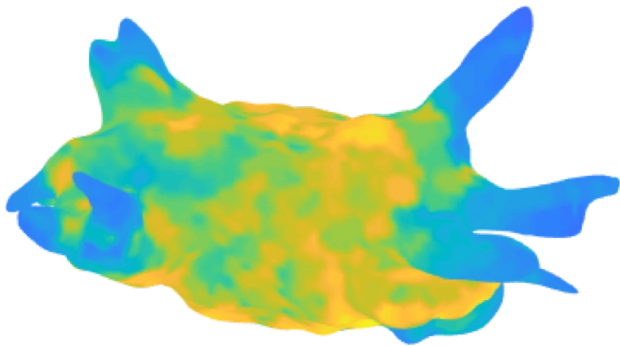
System used prior to ablation to map the patient left atrium

Rhythmia system (Boston scientific)



Activation time mapping,
and bipolar/unipolar electrogram voltage maps are acquired
(~20 min/patient)
The data are saved in a readable Matlab format for analysis

Electrical biomarkers are evaluated from the bipolar maps



Two electrical biomarkers:

1. Mean voltage $\langle V \rangle$
2. Slope of the histogram (VS)

Future:

- 24 regions of the atrium (regional statistics)
- Geodesic distance on the time activation maps (PhD thesis Leire Moriones)

We studied 122 patient maps (prior to ablation)

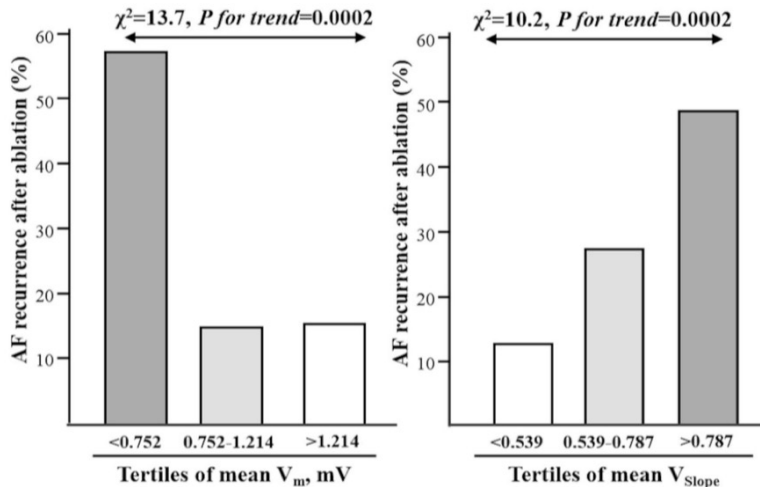
	A	B	C	D	E	F	G	H	I	J	K	L	M	N	O	P	Q	R	S	T				
1	name	NVERT	NFACES	AREA	MEDIA POT	Slope	R2	False media	dispersion	Q1	Q2	Q3												
2	pot<0,1	P<0,2	P<0,3	P<0,4	P<0,5	P<0,6	P<0,7	P<0,8	P<0,9	P<1	P<1,1	P<1,2	P<1,3	P<1,4	P<1,5	P<1,6	P<1,7	P<1,8	P<1,9	P<2				
3																								
4	F01_12_2015T09h08	7357	14513	137.3	0.7143	-0.9682 (0.0302)	0.956	0.7155 (0.912)	0.9460 (0.349)	0.1416	0.3492	0.9248												
5		0.1654	0.3522	0.4587	0.5387	0.6017		0.6494	0.6863		0.7168		0.7434	0.7668	0.7869	0.8059	0.8218	0.8375	0.8534	0.8661	0.8805	0.8914	0.9006	0.9103
6																								
7	F03_11_2015T09h58	7828	15470	145.31	1.0769	-0.4961 (0.0203)	0.926	1.0618 (1.587)	0.9393 (0.357)	0.1312	0.3573	1.4863												
8		0.1925	0.3767	0.4603	0.5219	0.566		0.5972	0.6222		0.6418		0.6607	0.6807	0.6979	0.7136	0.728	0.7406	0.7513	0.7634	0.7773	0.7869	0.7997	0.8109
9																								
10	F04_08_2015T13h08	7795	15440	147.52	0.1869	-1.8882 (0.1251)	0.847	0.1809 (0.290)	0.9554 (0.363)	0.0428	0.0801	0.1922												
11		0.5809	0.7589	0.8346	0.879	0.9091		0.9306	0.945		0.9562		0.9659	0.9727	0.9778	0.9815	0.9842	0.9873	0.9902	0.9926	0.994	0.9948	0.9965	0.9979
12																								
13	F05_11_2015T09h20	5068	9955	97.15	1.1941	-0.4625 (0.0208)	0.92	1.1807 (1.669)	0.9759 (0.361)	0.176	0.5399	1.5004												
14		0.1339	0.2749	0.3693	0.4337	0.484		0.5231	0.5619		0.5929		0.6297	0.6543	0.6787	0.7002	0.7175	0.7323	0.7499	0.7612	0.7743	0.7877	0.7999	0.8112
15																								
16	F09_09_T08h49	6989	13832	137.41	0.8219	-0.7329 (0.0289)	0.933	0.8191 (1.198)	0.9934 (0.375)	0.1176	0.2619	1.1075												
17		0.1674	0.4429	0.5233	0.5807	0.6235		0.6552	0.6803		0.702		0.7188	0.7336	0.7493	0.765	0.7784	0.7923	0.807	0.8199	0.8308	0.8419	0.8539	0.8652
18																								
19	F17_11_T14h51	7539	14836	143.93	2.0659	-0.4578 (0.0134)	0.96	2.0679 (2.401)	0.9701 (0.351)	0.1938	1.2555	3.033												
20		0.185	0.2531	0.3003	0.3326	0.357		0.3786	0.3998		0.419		0.4358	0.4559	0.4726	0.4896	0.5073	0.5252	0.5419	0.5584	0.5745	0.5904	0.6096	0.6245
21																								

Working hypotheses:

- 1) Low voltage areas correlate with scar tissue areas (see LGE-MRI studies)
- 2) Scar tissue (fibrosis) is prone to generate re-entry (arrhythmogenic substrate)
- 3) Heavily damaged LA is more susceptible to lead to “redo procedure” (probability)

→ Average potential and slope are the two “electrical” biomarkers of the LA !

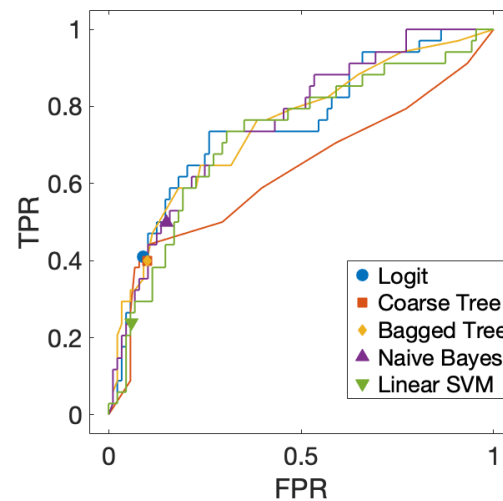
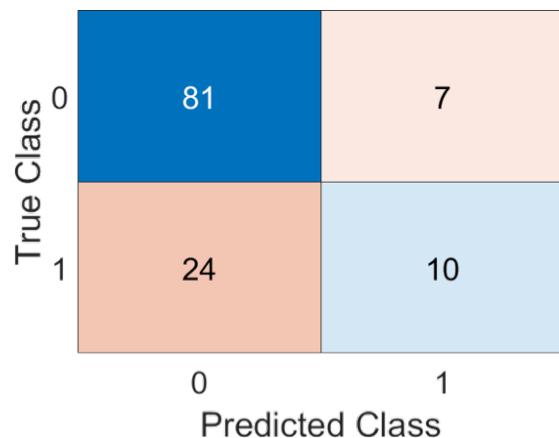
Main results of the map analysis



Results:

Both mean voltage (V_m) and VS are predictors of AF recurrence after ablation !

Logistic Regression is the best classifier given by the Matlab “classificationLearner” ML tool, (with a cutoff value of $V_m = 0.54$ mV).



Redo: 34/122 ≈ 28 %; Accuracy ≈ 75 %

Partial conclusions

- The average potential and the slope are good predictors for a repeat procedure at one year distance.
- More complicated statistical indicators are currently being tested,i.e., regional statistics and activation time maps.



ORIGINAL ARTICLE

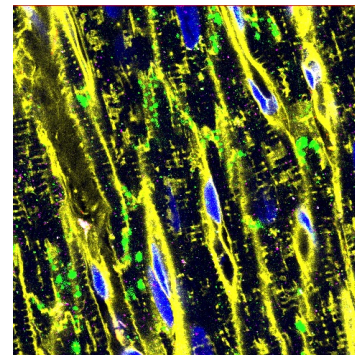
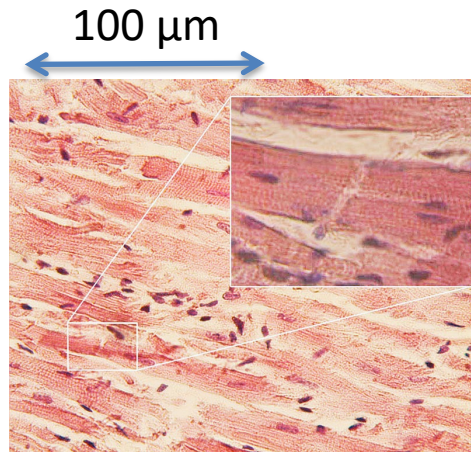
Association of left atrium voltage amplitude and distribution with the risk of atrial fibrillation recurrence and evolution after pulmonary vein isolation: An ultrahigh-density mapping study

Gabriel Ballesteros MD, Susana Ravassa PhD, Jean Bragard PhD, Pablo Ramos MD, Begoña López PhD, Enrique Vives MD, Renzo Neglia MD, Bernardo Wise MD, Arantxa González PhD ... See all authors ▾

First published: 11 May 2019 | <https://doi.org/10.1111/jce.13972>

IV) Wave propagation in the heart

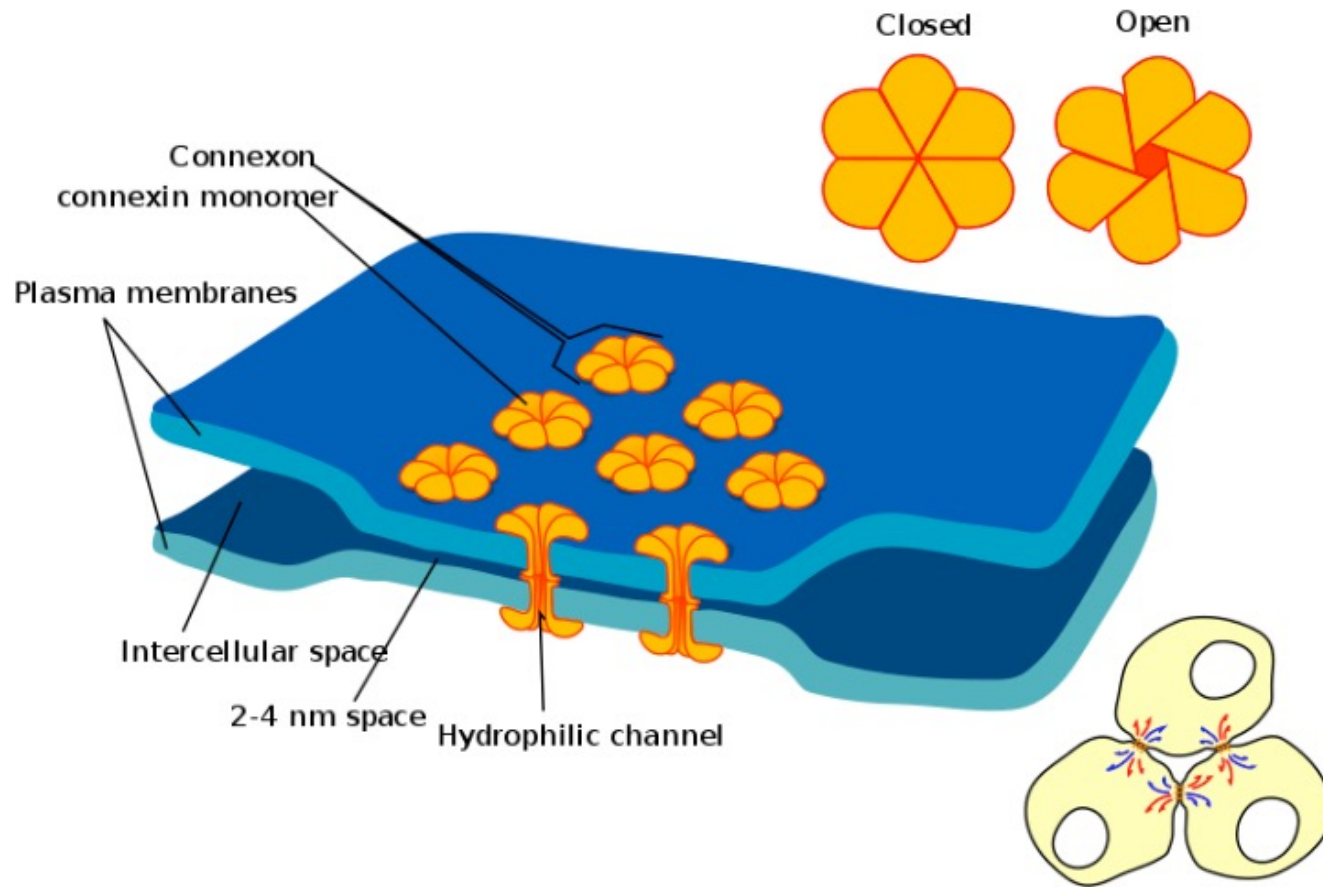
The structure of the cardiac muscle is complex and influences its electrical behavior and dynamics



- Wheat Germ Agglutinin (WGA)
- DAPI
- GJ (Connexin43)

The cardiac muscle is formed with cardiomyocytes, gap junctions (GJ), collagen and elastin fibers, fibroblasts, blood vessels,...

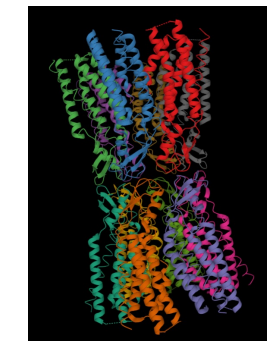
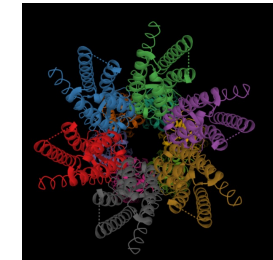
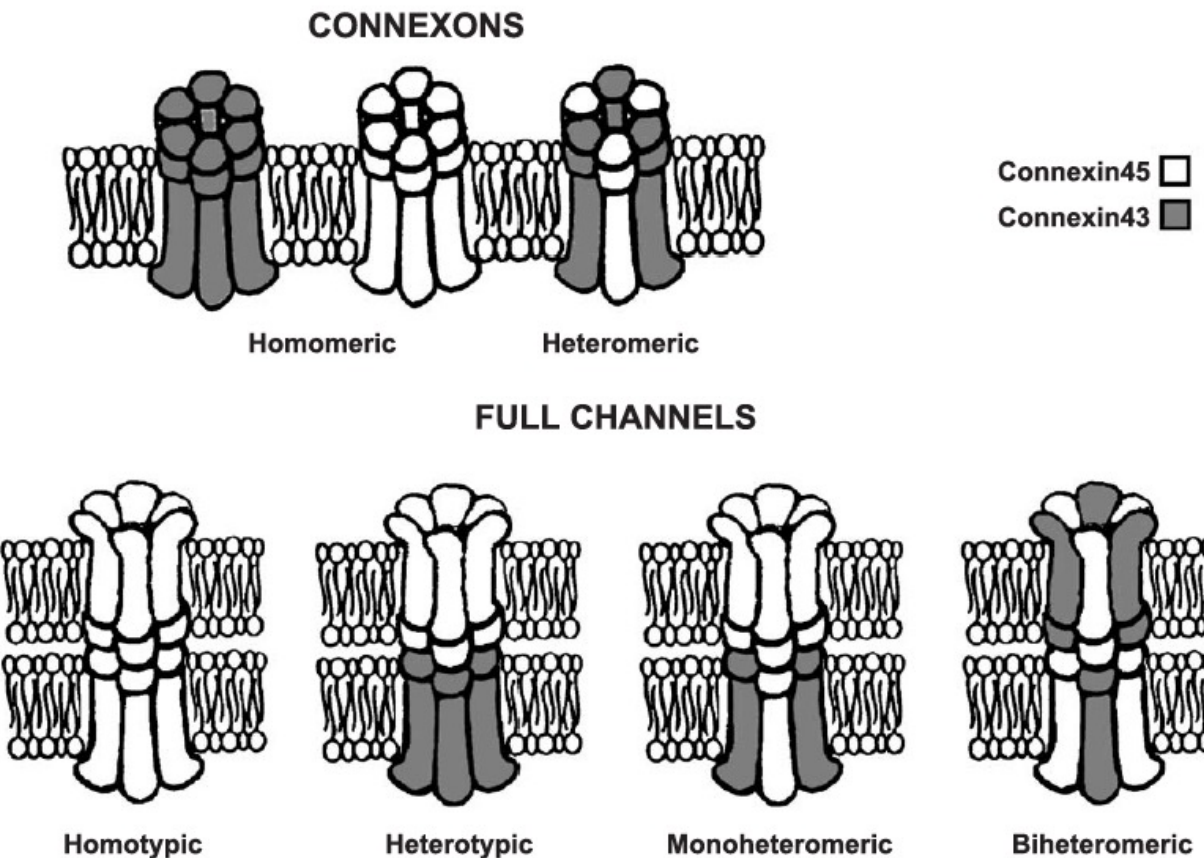
Gap junctions (GJ) are essential for the propagation of the electrical impulse AP from one myocyte to the next.



GJs form low electrical resistance passages between cardiomyocytes.

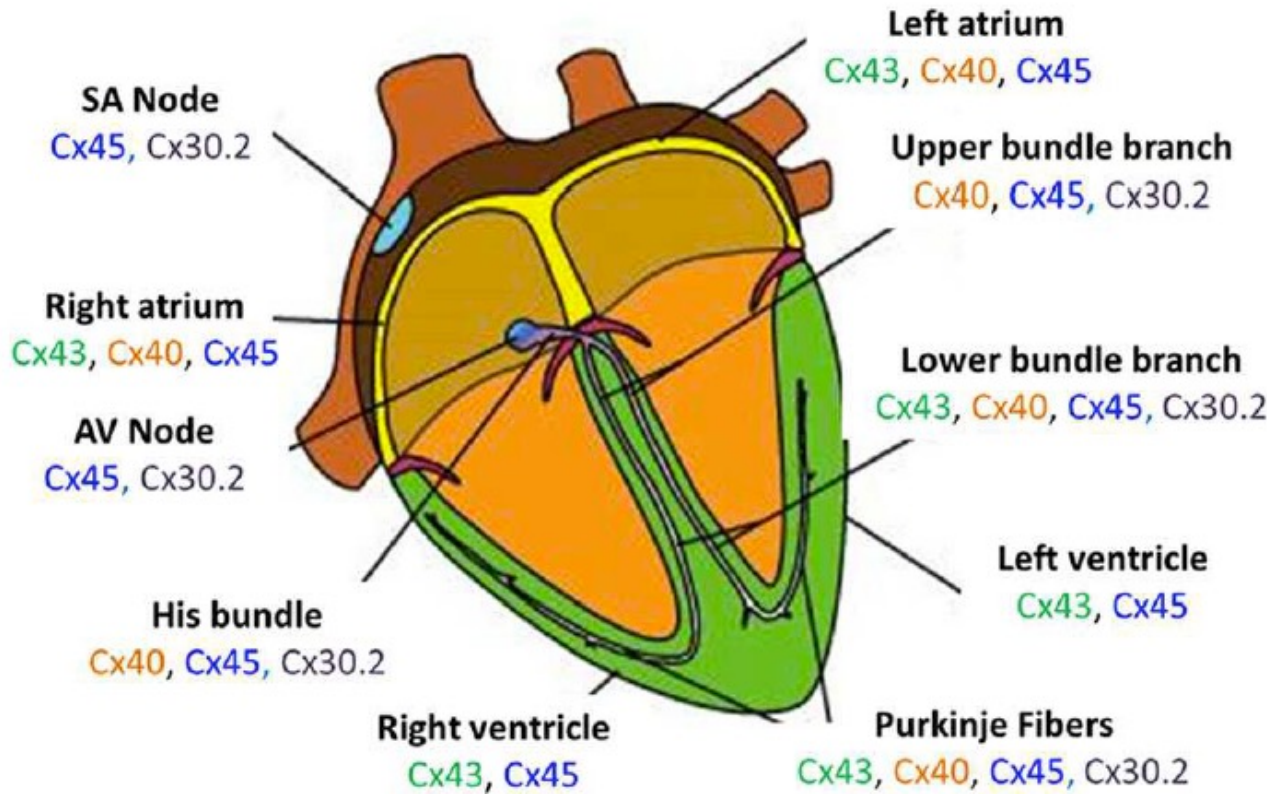
Source : Wikipedia

Different types of gap junctions (GJ) have been identified in the cardiac muscle



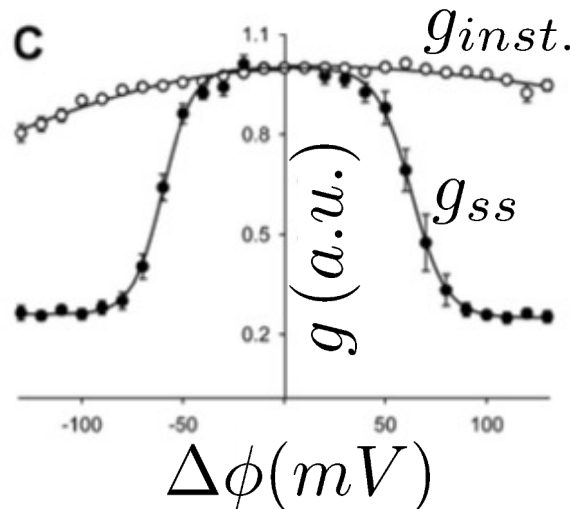
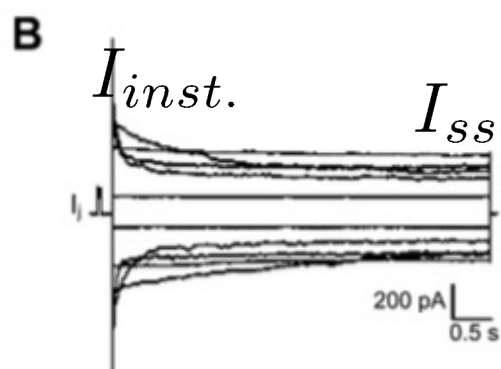
In cardiac tissue of mammalian, connexins type Cx40, Cx43 and Cx45 are the most common. The permeability of the GJ depends on its structure (g approx. 10 to 300 pS)

Different types of gap junctions (GJ) have been identified in the cardiac muscle (II)



The connexin's expression pattern varies in different location of the heart

Dual voltage-clamp method and whole-cell recording allow to measure the electrical properties of the GJ



a) Fix the membrane potential of both cells

$$\Delta\phi = V_2 - V_1 \quad \text{transjunctional voltage}$$

b) Measure the current between cells

$$I_{inst.} \quad I_{ss}$$

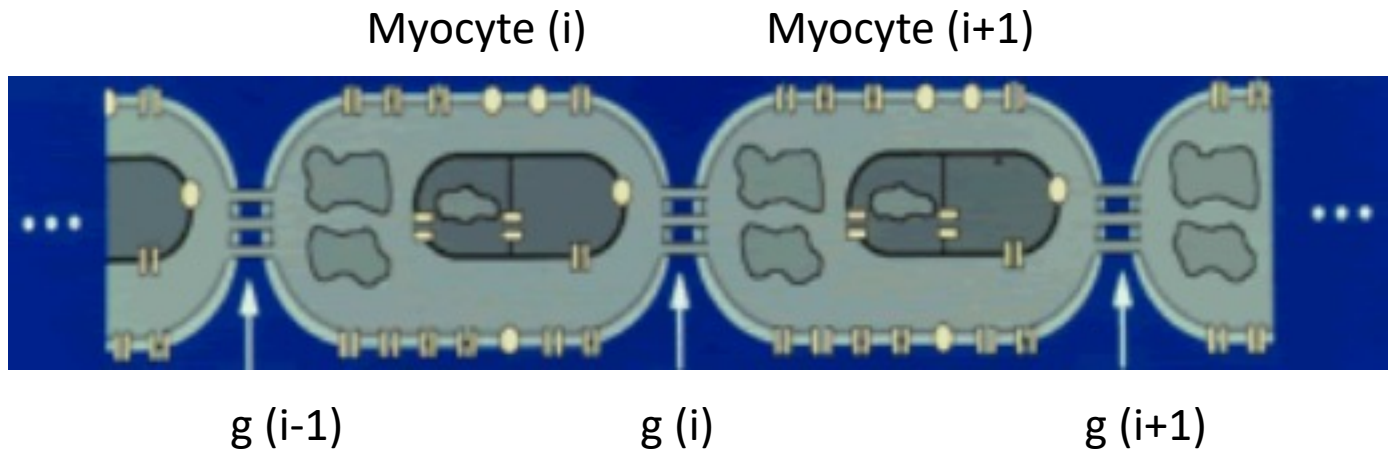
c) Calculate the normalized conductances

$$g_{inst.} = I_{inst.}/\Delta\phi \sim 100 \text{ } pS$$

$$g_{ss} = I_{ss}/\Delta\phi$$

The conductance between the two cells is a **dynamical variable**.

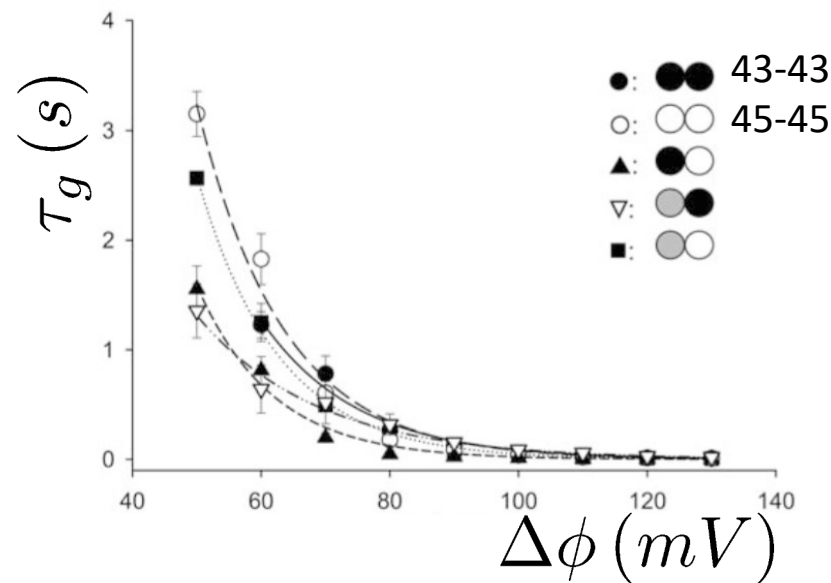
Mathematical model of a strand of cardiac tissue



1) Gap Junction's dynamics

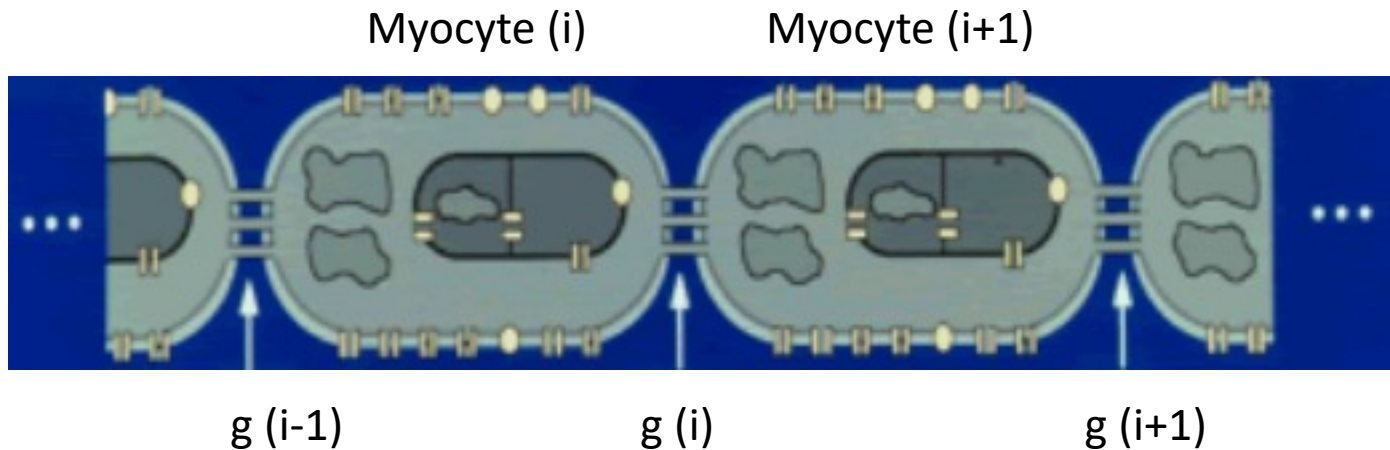
$$\frac{dg_i}{dt} = \frac{g_{ss}(\Delta\phi_i) - g_i}{\tau_g(\Delta\phi_i)}$$

$$\Delta\phi_i = V_{i+1} - V_i$$



The time constant τ_g is highly dependent of the connexin's transjunctional voltage

Mathematical model of a strand of cardiac tissue (ii)



2) Myocyte's transmembrane dynamics

$$\frac{\partial V}{\partial t} + \frac{I_{myo} + I_{ext}}{C} = \nabla \cdot (D \nabla V)$$

$$\frac{\partial \mathbf{s}}{\partial t} = f(V, \mathbf{s}) \quad \text{5 variables model (BCN)}$$

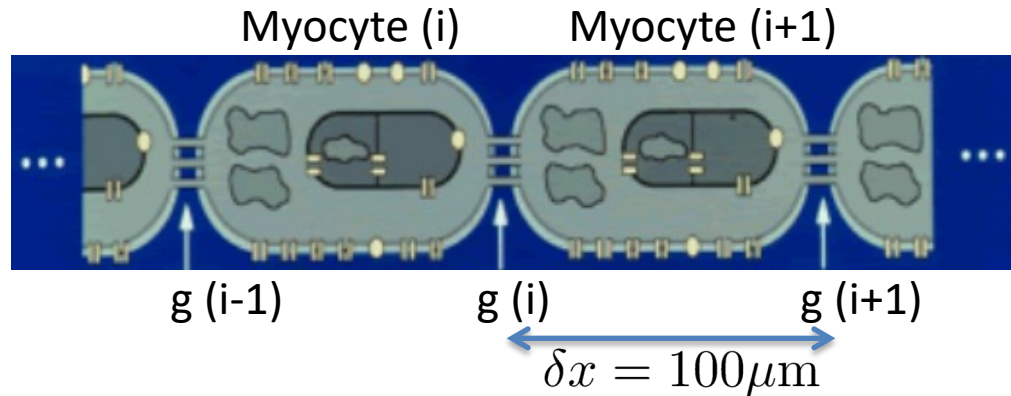
$$V = \phi_{intra} - \phi_{extra}$$

Monodomain approximation

$$D(x, t) = \bar{D} g(x, t)$$
$$\bar{D} = 1.5 \text{ cm}^2/\text{s}$$

- The gap junctions are the primary sites of membrane potential changes
- The entire myocyte cytoplasm becomes effectively iso-potential.

Numerical method



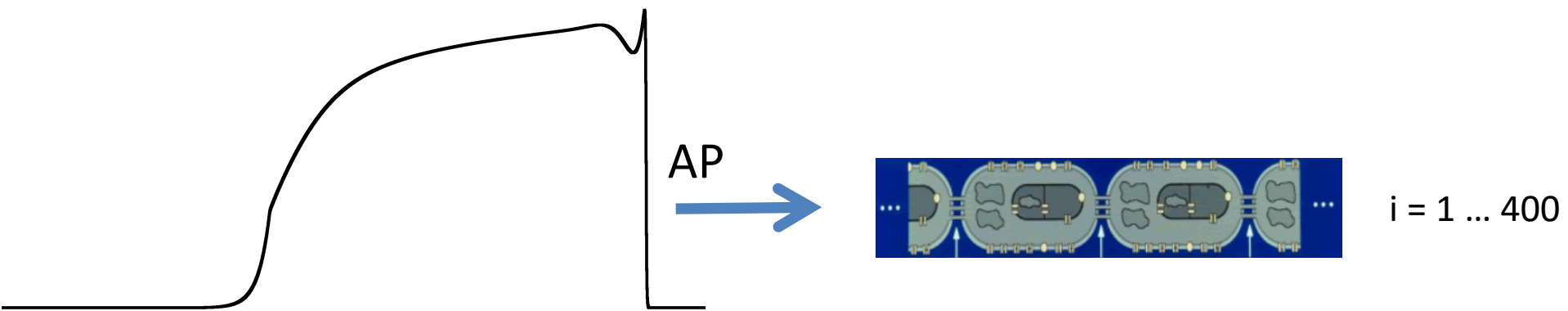
$$V_i^{(n+1)} = V_i^{(n)} + \bar{D} \frac{\delta t}{\delta x^2} \left\{ g_i^{(n)} \left[V_{i+1}^{(n)} - V_i^{(n)} \right] - g_{i-1}^{(n)} \left[V_i^{(n)} - V_{i-1}^{(n)} \right] \right\} - \delta t \frac{I_{myo}^{(n)} + I_{ext}^{(n)}}{C}$$

$$g_i^{(n+1)} = g_i^{(n)} + \delta t \frac{g_{ss}(\Delta\phi_i^{(n)}) - g_i^{(n)}}{\tau_g(\Delta\phi_i^{(n)})}$$

$\delta t = 10\mu\text{s}$ Integration time step

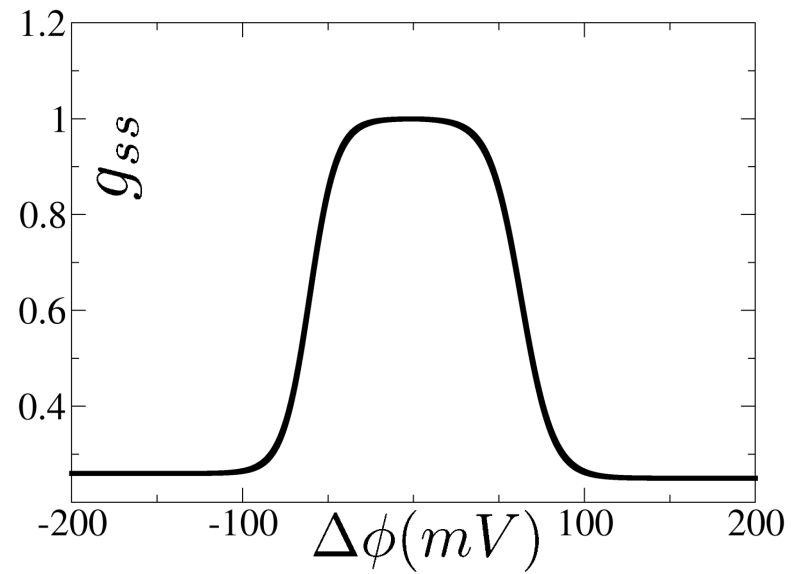
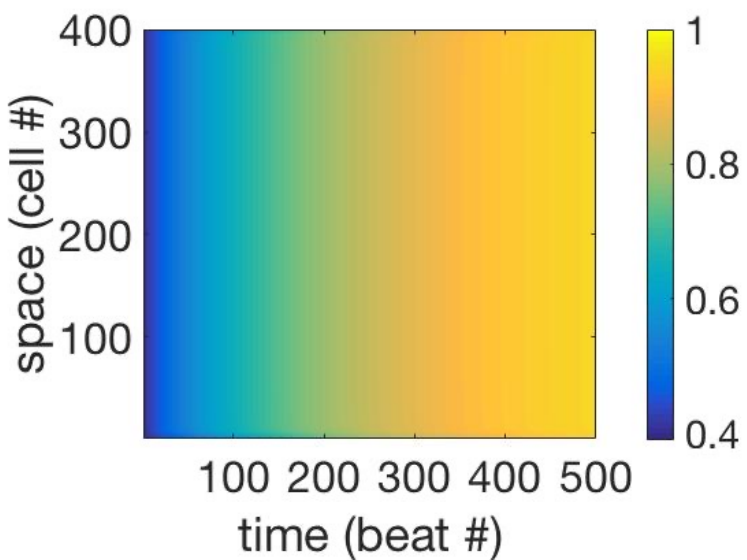
Super-index (n) refers to time step n. Subscript i refers to position i in the chain.

Stimulation protocol (L=400 cells)



1. Same initial values are set to all the GJ conductances ($g_i = g_{ini}$)
2. We excite the first 7 cells ($i=1..7$) to elicit an AP that propagates through the fiber
3. We repeat the stimulation with a period of $T = 480$ ms
4. We measure the time evolution of the GJ conductances after each stimulation

Results for the normal case (healthy)

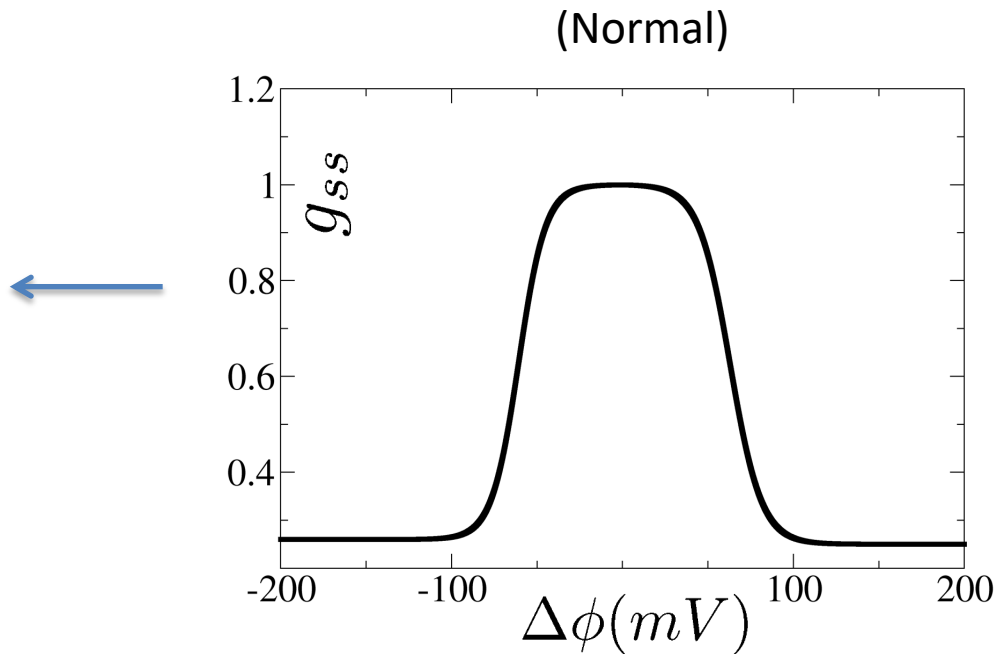
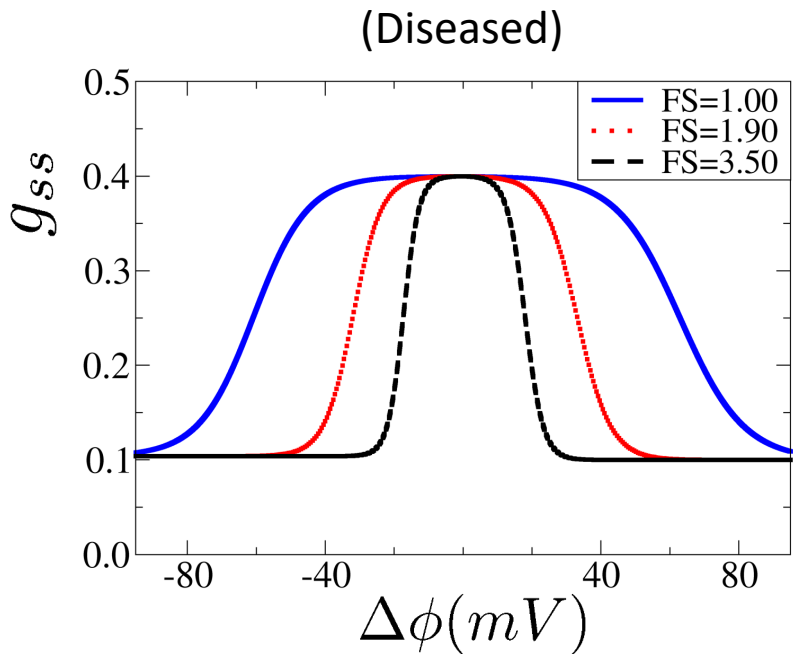


Here we set $g_{ini} = 0.4$

The conductances of all the GJ are returning to the max value $g \sim 1$

Nothing fancy happens !

Modification of the GJ dynamics (diseased case)

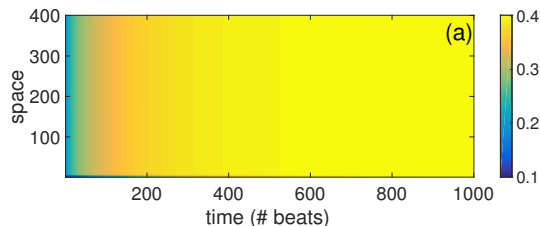


In order to model a diseased tissue we modify the characteristics of the GJ

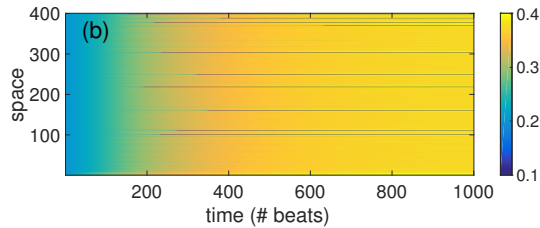
- We reduce the overall conductance to 40% of the normal values (ischemia)
- We introduce the ‘shrinking factor’ FS that alters the width of the plateau

Results of the GJ bistability induced by varying FS

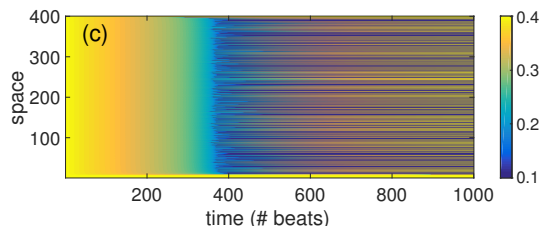
FS=1



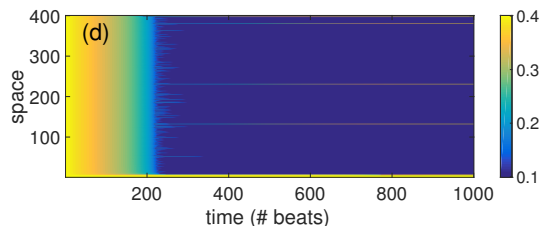
FS=1.44



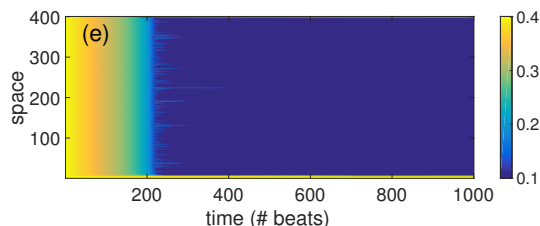
FS=1.9



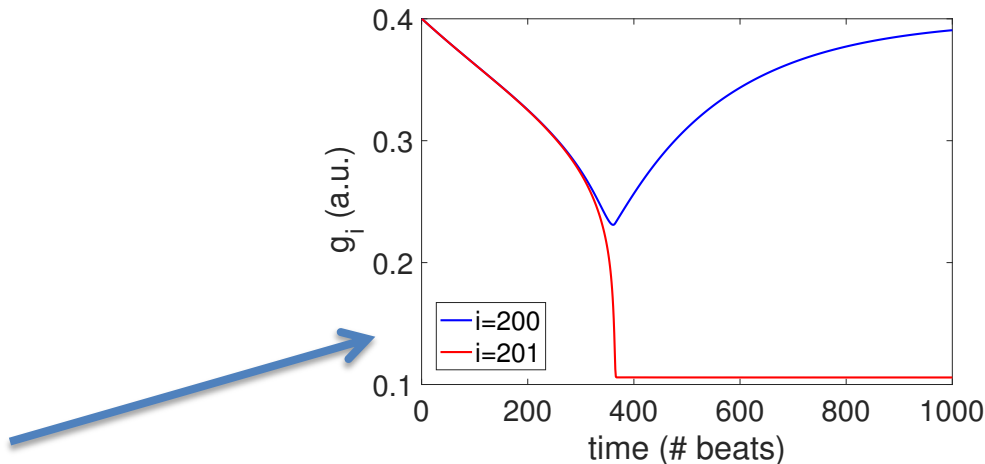
FS=3.5



FS=20

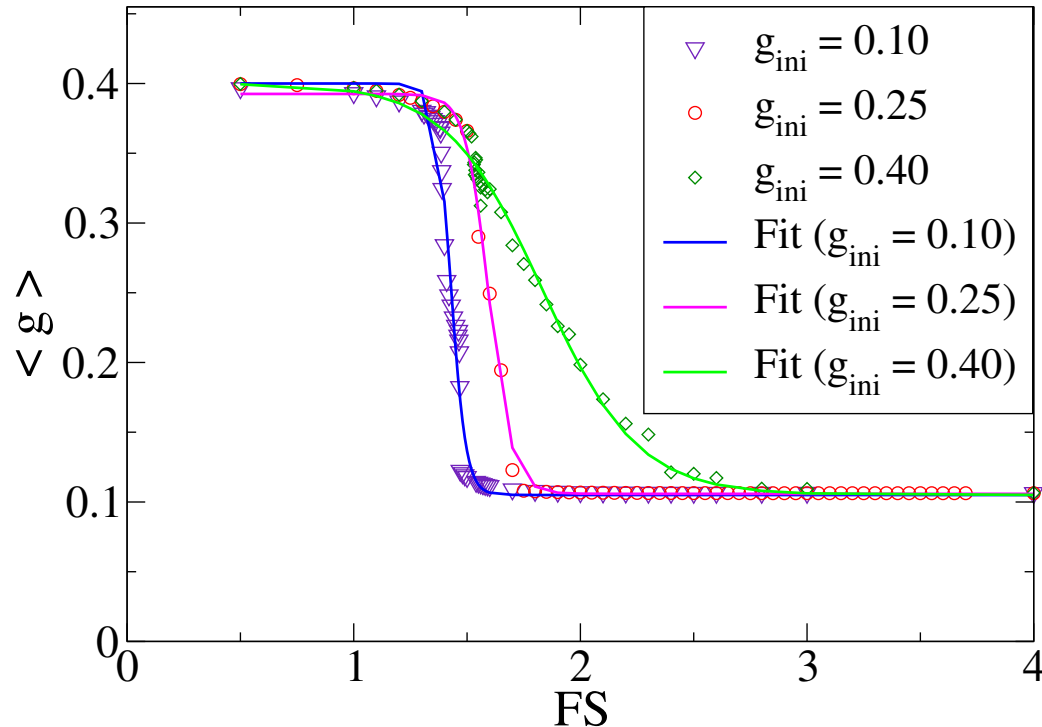


FS=1.9



We observe a transition by increasing FS from GJ conductance close to 0.4 (upper state) to GJ conductance close to 0.1 (lower state). For intermediate values of FS, we observe a spatially mixed state.

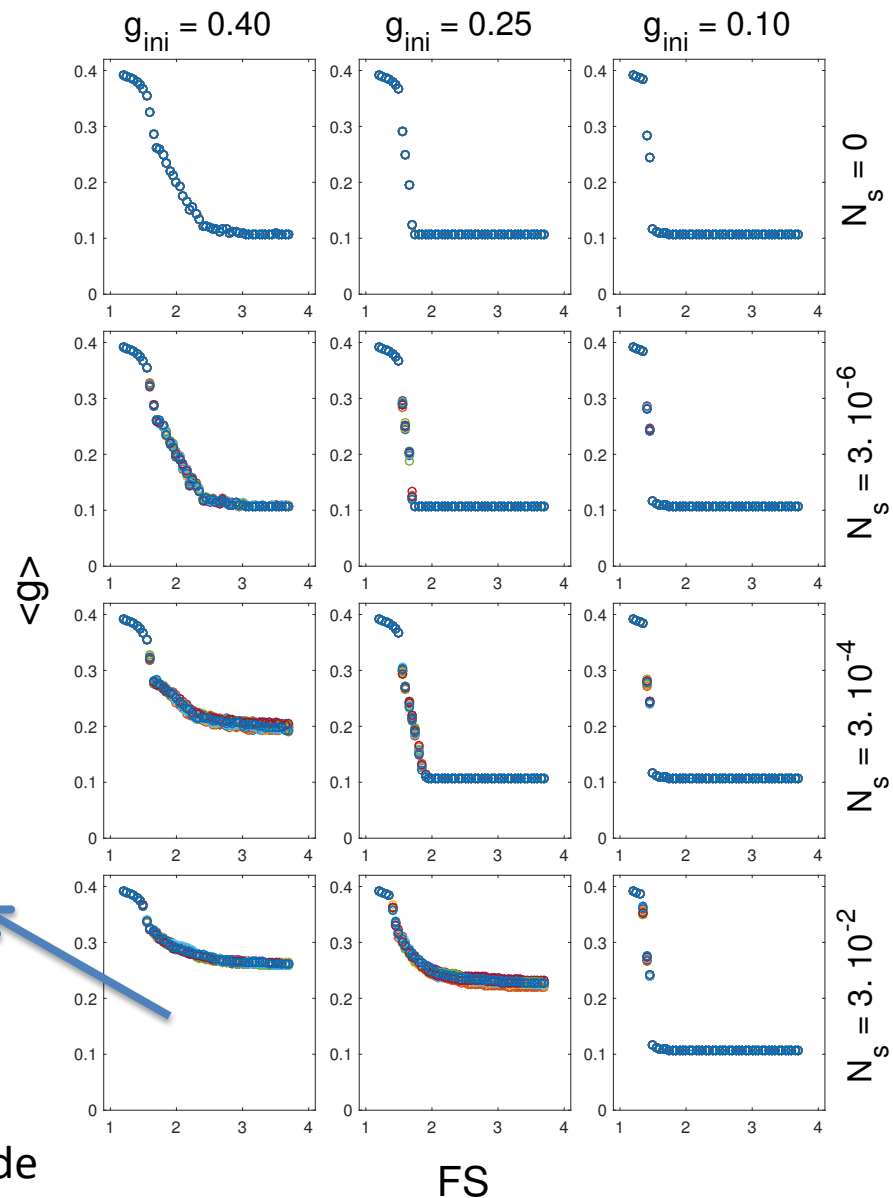
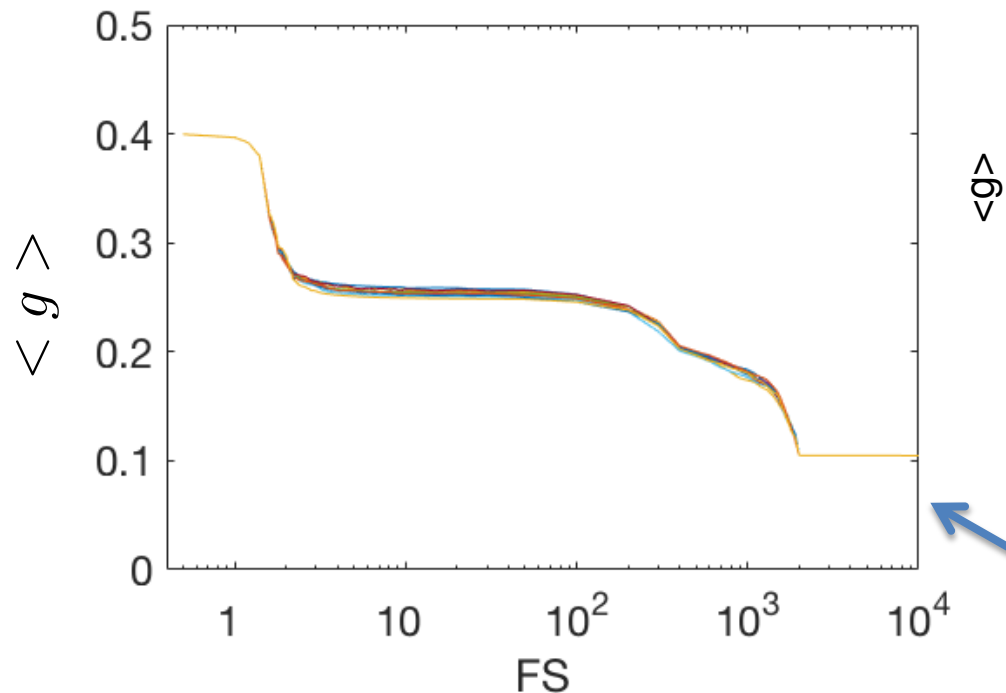
Study of the transition from UP to LOW GJ conductances



We have studied the influence of both FS and g_{ini} for characterizing the transition between upper and lower states of conductance. The spatial average of the conductance $\langle g \rangle$ is used as an **order parameter** to characterize this transition.

Influence of g_{ini} and added noise on the transition

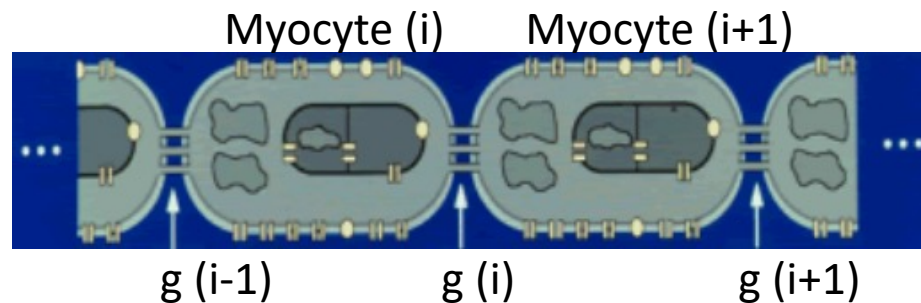
We have studied the influence of an initial added noise $g_i^{(0)} = g_{ini} + N_s \sigma_u$ to the transition.



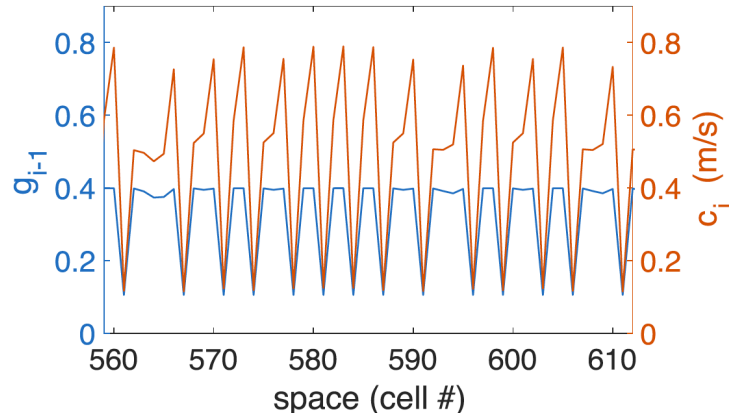
Persistent mixed state over 3 orders of magnitude

Non-homogeneous conductance induces dispersion in the AP conduction velocity

$$c_i = \frac{\Delta x}{\Delta t_i}$$

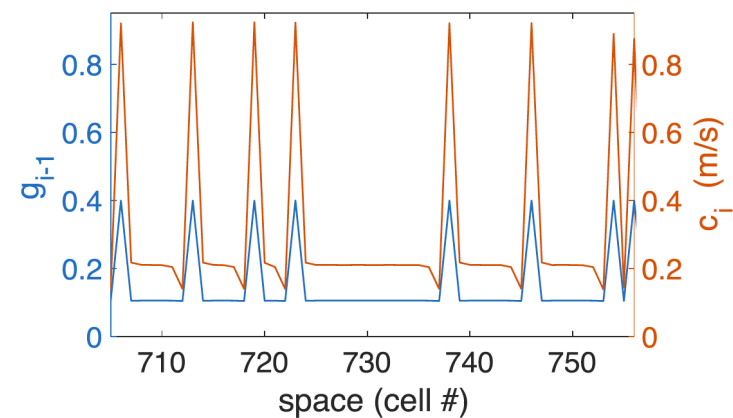


FS=1.61 ; $P_{up}=0.73$



$$\rho = 0.906$$

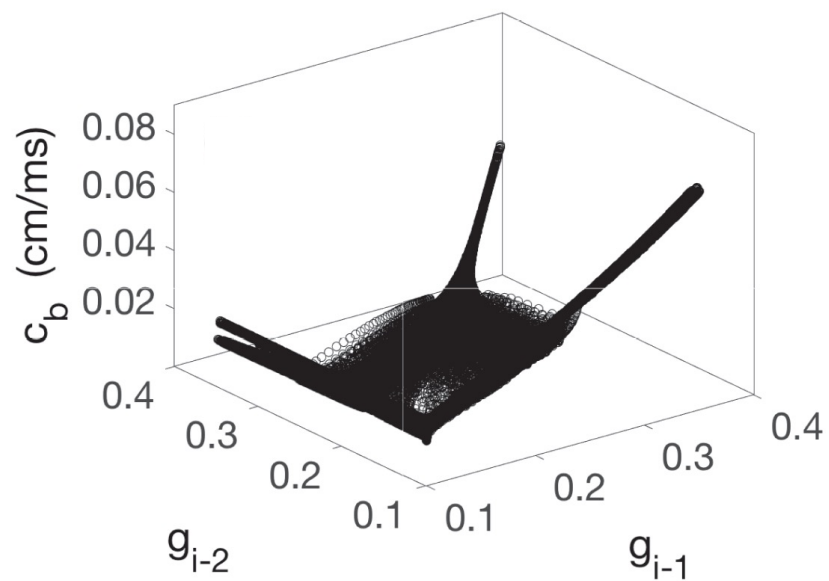
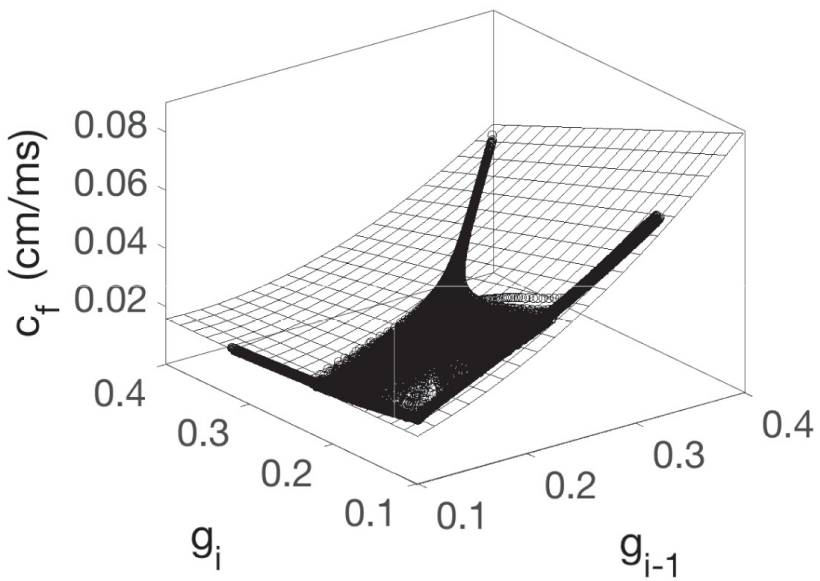
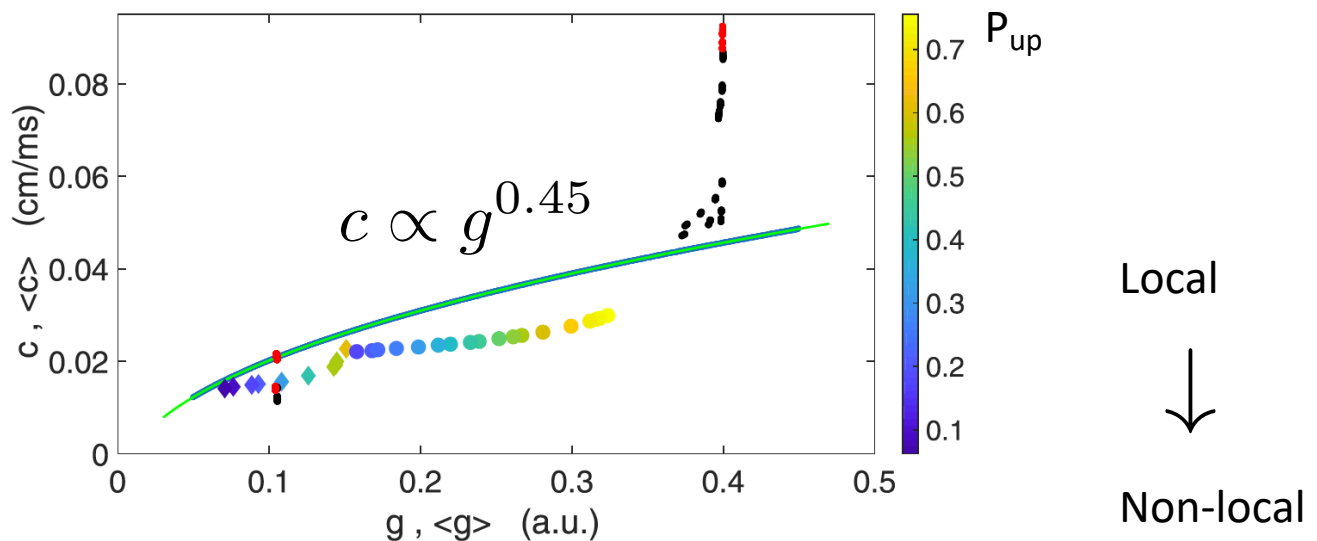
FS=2.19 ; $P_{up}=0.18$



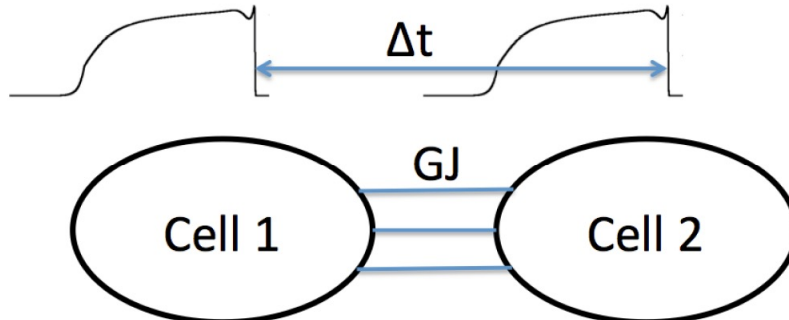
$$\rho = 0.996$$

- Local conductances and local conduction velocities are strongly correlated
- The relation is not strictly local !
- Propagation is from left to right !

Dispersion relations for the AP velocity



Stability of a single GJ

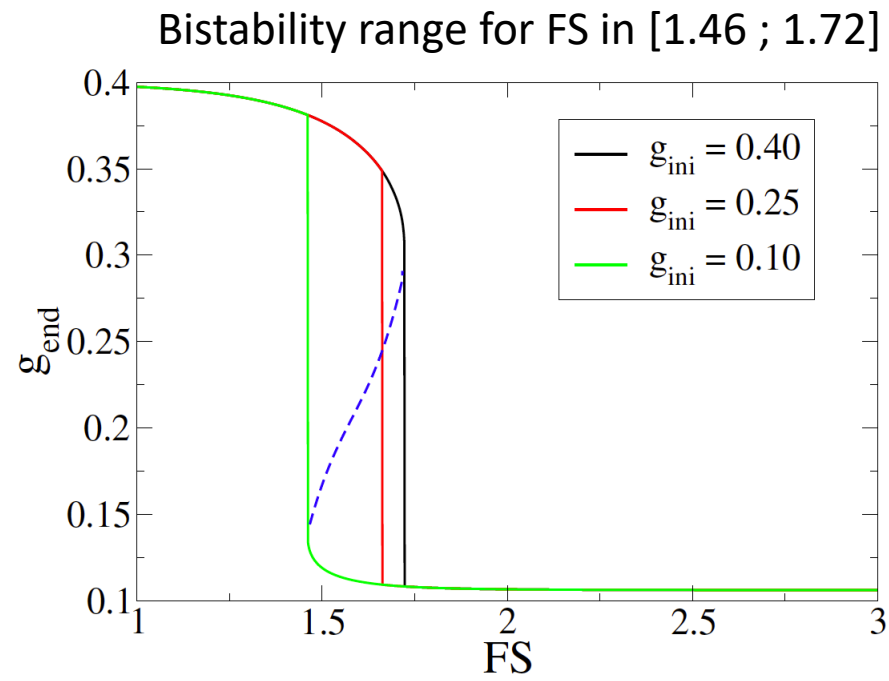
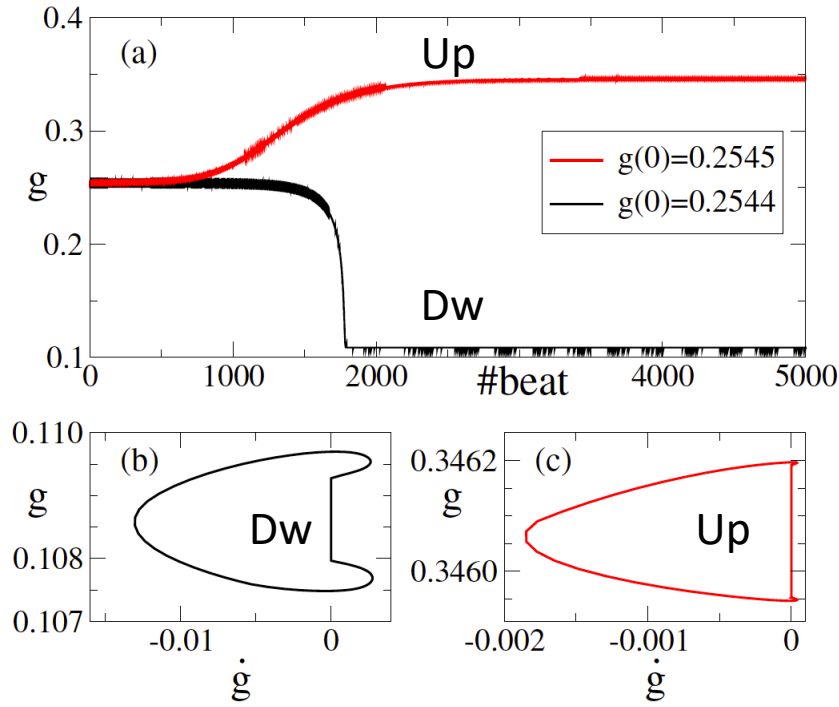


$$\frac{dg}{dt} = \frac{g_{ss}(\Delta\phi) - g}{\tau_g(\Delta\phi)}$$

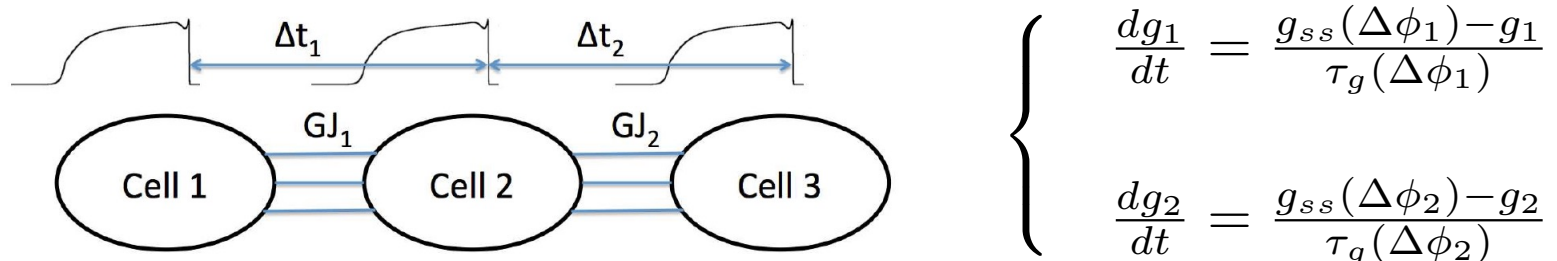
Kinematic relation: $\Delta\phi = \Delta V = V|_2 - V|_1 = V(t - \Delta t) - V(t)$

$$\Delta t = \frac{\delta x}{c(g)}$$

FS=1.67



Two coupled GJs

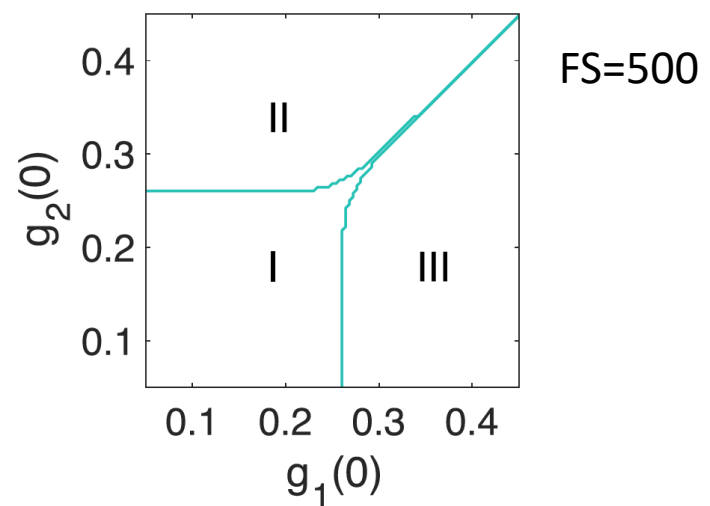
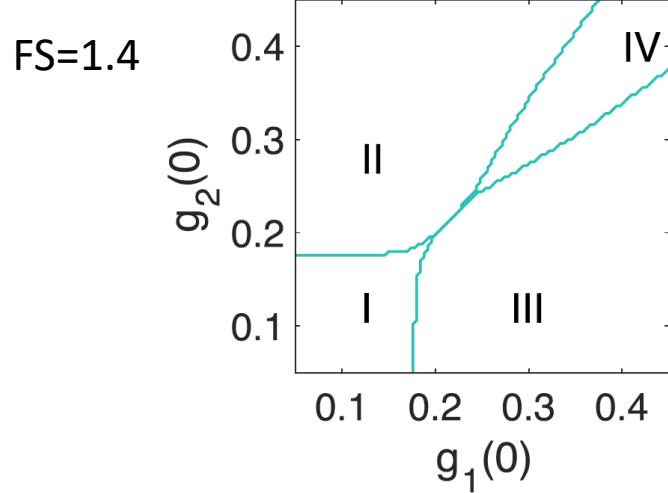


$$\frac{dg_1}{dt} = \frac{g_{ss}(\Delta\phi_1) - g_1}{\tau_g(\Delta\phi_1)}$$

$$\frac{dg_2}{dt} = \frac{g_{ss}(\Delta\phi_2) - g_2}{\tau_g(\Delta\phi_2)}$$

Kinematic relations: $\Delta t_1 = \frac{\delta x}{c_f(g_1, g_2)}$ $\Delta t_2 = \frac{\delta x}{c_b(g_2, g_1)}$

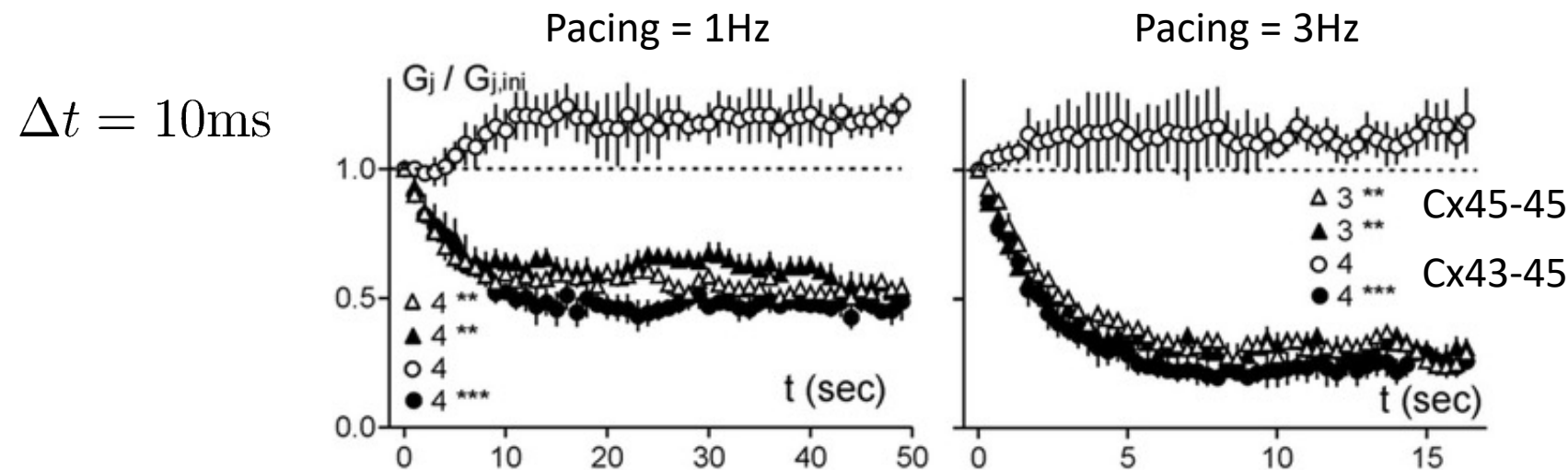
Attractor name	End g_1	End g_2	Local stability
Dw-Dw (I)	~0.1	~0.1	$1.24 < FS$
Dw-Up (II)	~0.1	~0.4	$0.985 < FS < 993.1$
Up-Dw (III)	~0.4	~0.1	$0.985 < FS < 993.1$
Up-Up (IV)	~0.4	~0.4	$FS < 1.665$



Related experimental study showing bistability for GJ

Junctional delay, frequency, and direction-dependent uncoupling of human heterotypic Cx45/Cx43 gap junction channels

Willy G. Ye ^{a,1}, Benny Yue ^{a,1}, Hiroshi Aoyama ^b, Nicholas K. Kim ^a, John A. Cameron ^a,
Honghong Chen ^a, Donglin Bai ^{a,*}



By varying the junctional delay Δt and the pacing frequency, they observe a different dynamics for the GJ conductances. It is also highly dependent on the GJ composition.

Partial conclusions

- We have studied the conductance dynamics of the GJ in a 1D model
- In some simulated diseased situations we observe bistability in the values of the GJ conductances.
- The high to low level of conductance is mediated by parameter FS.
- In the intermediate mixed state we observe a highly alternating spatial distribution of the GJ conductances.
- A simple stability analysis of the GJ dynamics explains the observations.
- Future Plan: Connect our findings to electrophysiology experiments

Acknowledgements

Collaborators:

UNAV-CIMA-CUN (Dr. Javier Diez, MD, Dr. I. Garcia-Bolao, MD, ...)

UPC Barcelona (B. Echebarria, A. Peñaranda,
I.R. Cantalapiedra, E. Alvarez-Lacalle)

Liege University (P.C. Dauby, A. Collet, ...)

Utah CVRTI (F.B. Sachse, A.C. Sankaranikutty, ...)

Max Planck Göttingen (A. Witt, S. Luther,...)

UNAV_Farma: Prof. I.F. Troconiz

Madrid_Ophtalmo. : Dr. M. Ibarz

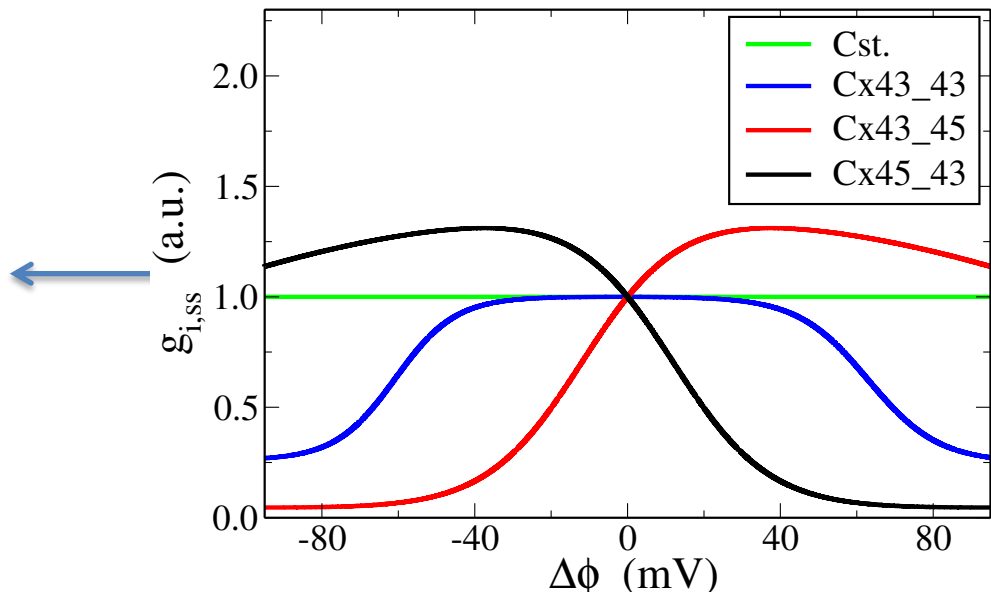
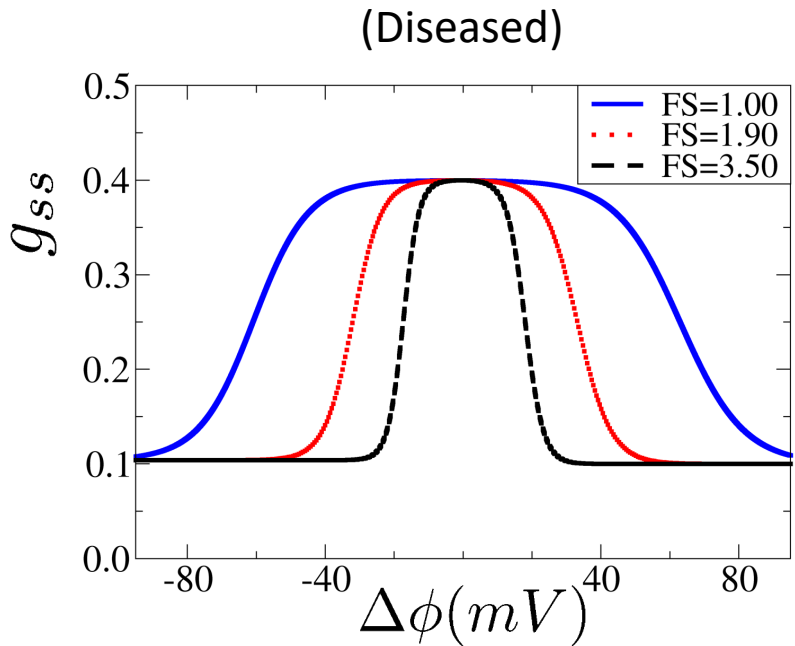
Financial support : (MINECO) under grant number PID2020-116927RB-C22
(Spain research grant)

Thank you !

1997 Summer School & Workshop/Curso de verano, Gulbenkian International Advanced. Course
INTRODUCTION TO DYNAMICAL SYSTEMS: THEORY FOR BIOSCIENCE.



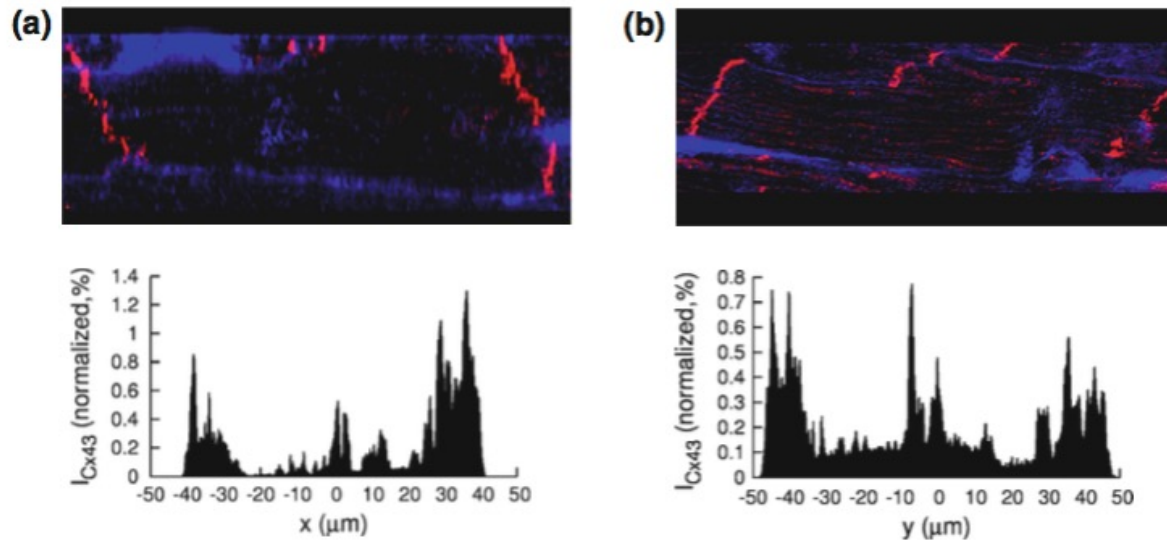
Justification of the FS factor



Heterotypic GJs have asymmetrical g_{ss} functions.

A mix of several type of GJ types may justify the FS parameter

Justification of the introduction of noise (Ns)



Spatial heterogeneities and different geometric orientation
lead to variability in the GJ conductance
This may justify the noise factor